JIMMA UNIVERSITY

JIMMA INSTITUTE OF TECHNOLOGY

SCHOOL OF GRADUATE STUDIES

FACULTY OF MECHANICAL ENGINEERING

DESIGN OF MECHANICAL SYSTEM ENGINEERING

ANALYTICAL AND NUMERICAL ANALYSIS OF MIXED-MODE I/II FATIGUE CRACK GROWTH RATE AND PATH PREDICTION

A Thesis submitted to School of Graduate Studies of Jimma University in Partial Fulfillment of the Requirements for the Degree Master of Science in Design of Mechanical System

By

Derara Umeta Dina

March 11, 2021

Jimma, Ethiopia

JIMMA UNIVERSITY

JIMMA INSTITUTE OF TECHNOLOGY

SCHOOL OF GRADUATE STUDIES

FACULTY OF MECHANICAL ENGINEERING

DESIGN OF MECHANICAL SYSTEM ENGINEERING

ANALYTICAL AND NUMERICAL ANALYSIS OF MIXED-MODE I/II FATIGUE CRACK GROWTH RATE AND PATH PREDICTION

A Thesis submitted to School of Graduate Studies of Jimma University in Partial Fulfillment of the Requirements for the Degree Master of Science in Design of Mechanical System

Main Advisor: Prof. Hirpa G. Lemu

Co-Advisor: Mr. Iyasu Tafese

Declaration

I hereby declare that the work, which is presented in this thesis entitled "**Analytical and Numerical Analysis of Mixed-Mode II Fatigue Crack Growth Rate and Path Prediction**" is my original work. Has not been presented for a degree in any other university, and that all sources of material used for this thesis have been duly acknowledged.

Derara Umeta _____ _____

Signature Date

Approval

As a member of the examining board of open defense, we have checked and evaluated the Master's Thesis prepared and presented by **Derara Umeta** entitled "*Analytical and Numerical Analysis of Mixed-Mode II Fatigue Crack Growth Rate and Path Prediction*". Hereby we certify this work fulfilled the requirement of the Degree of Master of Science in Mechanical Engineering (Design of Mechanical System).

1. Department Chairman: Mr. Iyasu Tafese (MSc)

Signature: _____ Date: _____

2. Main Advisor: Prof. Hirpa G. Lemu (PhD)

Signature:__Hirpa_____Date:__07/09-2021.___

3. Co-Advisor: Mr. Iyasu Tafese (MSc)

Signature: _____Date: _____

4. Internal examiner:

Signature: _____Date: _____

5. External examiner:

Signature: _____Date: _____

Abstract

Mode I fracture mechanics have been relatively mature, but mixed-mode fracture mechanics present challenges under different loading angles. Since most engineering materials are subjected to inclined cracks and/or multiaxial loading, there is a well-justified need to establish a solid understanding of their fracture behavior under mixed modes. This thesis aims to study how to predict mixed-mode fatigue crack propagation under various loading angles for the compact tension shear specimen of 7075-T651 aluminum alloy. In this study, both analytical and finite element approaches were used to predict the expected fatigue crack growth rate and direction for various models. Equivalent stress intensity factor was analyzed considering the most common approaches such as Irwin, Tanaka, Richard, and Demir criterion. A comparison between them was performed taking into account how to examine which fatigue crack model of mixed-mode can better predict fatigue crack growth rate close to the experimental data obtained from the literature. To achieve this, predicted equivalent stress intensity factor (concerning the experimental stress intensity factor) for each of the four models for 30°, 45°, and 60° loading angles were considered. Tanaka criterion is in good agreement with the experimental results up to 45° *loading angle. Although the Demir model is expected to provide higher accuracy for higher mode mixity cases, its prediction is close to the experimental data even for the case of loading angle equal to both* 30° *and* 45°*. Overall, Demir's models predict crack propagation rate close to the selected experimental data based on the overall consistent performance.*

Keywords: Mixed-mode; Fatigue crack growth; Compact tension specimen; Numerical modeling

Acknowledgments

All glory and honor to Almighty God, who gave me the courage and strength to successfully finish such a monumental task. Next, I want to express my thanks to Prof. Hirpa G. Lemu, my principal supervisor, for initiating and supervising this thesis, as well as providing me with the required direction, constant supervision, collaboration, and inspiration during this research. Then, I'd want to convey my deepest gratitude to Mr. Iyasu Tafese, my associate supervisor, for his professional supervision during my studies. He was really helpful in the completion of this thesis.

Finally, and most importantly, I want to convey my heartfelt gratitude to my family for their unwavering encouragement, patience, and unwavering support during my studies. I express my heartfelt gratitude to everyone who helped me during this research for their unfailingly kind support and assistance.

Table of Contents

List of Figures

List of Tables

List of Acronyms

CTS	Compact Tension Specimen
EPFM	Elastic-Plastic Fracture Mechanics
FE	Finite Element
FCG	Fatigue Crack Growth
FCGR	Fatigue Crack Growth Rate
JIT	Jimma Institute of Technology
LEFM	Linear Elastic Fracture Mechanics
MERR	Maximum Energy Release Rate
MTS	Maximum Tangential Stress
SED	Minimum Strain Energy Density
SIF	Stress Intensity Factor
SMART	Separating Morphing and Adaptive Remeshing Technology
UMM	Unstructured Mesh Method
XFEM	Extended Finite Element Method
VCCT	Virtual Crack Closure Technique

List of Symbols

Δa	Crack to grow in length by a specific amount
B	Plate thickness
C	Material-dependent Paris constant
da	Crack increment
dA	Increase in crack area
E	Total Energy
F	Uniaxial force applied to the loading device
G	Energy release rate
G_c	Critical value of energy release rate
G_I	Mode I energy release rate
G_{II}	Mode II energy release rate
G_{III}	Mode III energy release rate
ΔK	Stress Intensity Range
ΔK_{eq}	Equivalent stress intensity factor
K_I	Mode I stress intensity factor
K_{IC}	Fracture toughness
K_{II}	Mode II stress intensity factor
K_{III}	Mode III stress intensity factor
ΔK_{th}	Threshold tress intensity factor range
m	Material-dependent Paris exponent
N	Number of Cycles

r	Crack tip radius
R	Stress ratio
S	Strain energy density
w_f	Fracture energy
W_s	External forces
θ_0	Crack initiation angle
ϕ_0	Crack deflection angle
v	Poison ratio
Π	Potential Energy
Π_o	Potential energy of an uncracked plate
γ_p	Surface energy of the material for ductile materials
γ_s	Surface energy of the material for brittle materials
σ	Nominal sress
σ_c	Critical stress
σ_y	Yield stress

CHAPTER 1 Introduction

1.1. Background

Fatigue cracks are very common in mechanical components exposed to huge cyclic loads. The mere presence of a crack doesn't regularly risk the structural integrity of a component or a structure. It is, in any case, necessary to know the rate and the mechanisms of the crack growth as well as the time required for an initial micro-crack to grow up to a critical size, at which the integrity of the component or structure would be debilitated [1]. The damage tolerance concept is widely used in modern aircraft design to ensure flight safety, which has predicted fatigue crack propagation of lives of aircraft components under service loading necessary [2].

Cracks are close detachments of a structure's substance. The force flaw in the component is significantly disrupted by these material separations. The force flaw is abruptly diverted, resulting in the formation of a local single stress field in the fracture tip or crack front. The transfer of forces or stresses through a component is known as force flaw. Force flaw lines can also be understood as stress level lines. High local stresses occur when force flaw lines are sharply redirected and lie close to each other [3].

A crack is considered as a mathematical section due to the simplicity of its geometry, and in fracture mechanics, there are three fundamental crack loading types (loading modes) for all fractures that form in components and structures. Those are Mode I (encompasses all normal stresses that cause the crack to open), Mode II (associated with all shear stresses that engender opposed sliding of the crack surfaces in the direction of the crack), and Mode III (corresponds to the non-plane shear stress state) [3, 4]. Figure 1.1 illustrates these three crack modes [5].

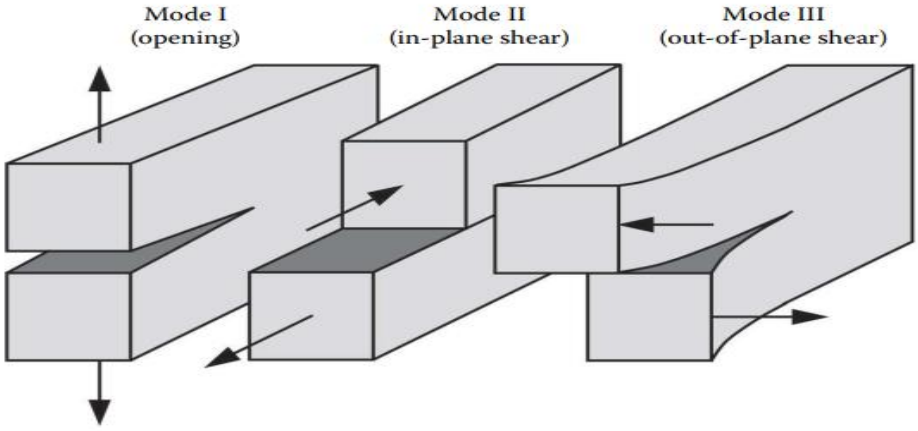

Figure 1.1: The three modes of loading that can be applied to a crack.

A crack propagates as one of the three basic failure modes or as a mixed-mode under applied load conditions [6]. Mixed-mode conditions are any combinations of these three modes. Research generally shows that many materials fail in mixed-mode conditions. They fail mainly in combinations of mode I and mode II. Focusing initially on mode-I fracture problems, Fracture Mechanics concepts have been developed and applied to practical engineering problems successfully to assess the safety and damage tolerance of structures over the past six decades [7]. There are still many fracture issues and phenomena that need to be solved in the fracture mechanics sector. The mode I mechanism of failure, in particular, has received a lot of attention thus far. Despite this, many failures occur under mixed-mode loading circumstances, particularly in their early stages [8].

The fracture criteria for mixed-mode cracks are currently being developed around two aspects: crack growth conditions and crack growth direction [9]. To explain the two main aspects, the researchers explained the macro-fracture mechanism from various perspectives and established corresponding mixed-mode fracture criteria. It has been revealed that there are two different fracture failure mechanisms for I-II mixed-mode cracks, namely the tensile-type fracture mode and the shear-type fracture mode [9]. In many engineering problems faced today, mixed-mode fracture conditions are encountered due to different reasons; multi-axial and mixed-mode loads, the non-perpendicular orientation of crack surfaces concerning uniaxial loading, and different types and combinations of boundary conditions. Thus, a thorough understanding and knowledge of mechanisms driving mixed-mode fracture and crack growth conditions are necessary for the accurate assessment of such

conditions computationally and experimentally. Although initial studies on the extension of an in-plane mixed mode crack can be traced back to five decades [10].

The direction of the applied load may change in practice, and it would be unnecessarily restrictive to suppose that the load and crack should always be kept normal to one another. Because of the absence of geometric symmetry, the majority of failures in service are of the mixed-mode type, in which the fracture does not spread in the direction normal to the applied stress. This impact must be taken into consideration when predicting fatigue crack propagation, and it has been found to have a substantial role in cracks that begin under monotonic stress [11]. Problems of this type are encountered in multi-phase materials such as welded structures, adhesive joints, composite materials, plain and reinforced concrete structures, bridges, aircraft, and so forth. A mixed-mode interaction can also develop when crack branching occurs, which occurs when a crack changes direction and the traditional Griffith energy balance can no longer be used since cracking is not collinear. Cracks in the skin of aircraft fuselages can also occur and be exposed to mixed-mode fracture conditions. In general, crack initiation and propagation in a complex state of stress must be connected to the stress intensity factors that regulate it.

In addition, an accurate evaluation of stress intensity factors (SIFs) is very fundamental for the prediction of failure and crack growth. To evaluate the SIF of a cracked component, numerical tools such as finite element method (FEM) [12], boundary element method [13], and extended finite element method (XFEM) [14], [15] are available. Out of these numerical methods, the extended finite element method is the most successful and powerful numerical method for solving a variety of engineering and science problems [16], [17]. This method naturally lends itself to FCG, where a crack propagates along with a solution-dependent path, independent of the mesh. Extensive work was done to develop efficient models to evaluate the FCG and fatigue life in order to prevent fatigue failures. Despite the fact that, the Finite Element (FE) method is widely utilized in structural design, most commercial FE codes do not provide fatigue analysis directly [18]. To conduct fatigue predictions, additional plug-ins or toolkits are required and these toolkits are designed for the commercial FE software ANSYS and ABAQUS. There are numerous experimental models that have been presented, however, doing the processes is typically time-consuming and costly. The numerical analysis and use

of an expanded finite-element method used in the simulation is an effective means of reducing experimental effort, time, and expense [19].

Engineering simulation of fracture during the design phase to predict a product's toughness has been an available alternative method since the early 1980s. However, simulation of fracture has not been easy to set up and perform until now. Traditionally, the meshing stage consumed a lot of time (up to several days) because engineers had to fit a crafted mesh involving hexahedrons (hex) and wedges to capture the crack front the ideal mesh using only hex elements was often not possible. This led engineers to simplify the geometry of the crack to fit a hex-only mesh pattern, resulting in loss of fidelity in fracture analysis.

Engineers can now reduce preprocessing time by using Unstructured Mesh Method (UMM) automatically generated all-tetrahedral (tet) mesh for crack fronts, while still achieving the same high-fidelity results as a simulation run with the ideal hex mesh configuration, thanks to the new UMM in ANSYS Mechanical. The time it takes to mesh has been lowered from many days to just a few minutes. ANSYS Mechanical now features the Separating Morphing and Adaptive Remeshing Technology (SMART) crack growth simulation technology, which allows for automated remeshing during simulations, due to UMM. With a few clicks, a SMART simulation may be set up, eliminating the need for lengthy preprocessing sessions [20].

This thesis focuses on conducting fatigue life prediction of mixed-mode I/II fatigue crack growth using various equivalent stress intensity factor models using the CTS specimen geometry. To this aim an XFEM is coupled with the Paris Law and implemented in ANSYS software is used to study the effect of the loading angle for the CTS specimen with different initial cracks and with different loading angles. Finally, the performance and capability of various models is assessed by comparing the predicted life to analytical and the experimental result from the literature.

1.2. Statement of the Problem

Under linear elastic fracture mechanics (LEFM) analysis, the SIFs are used to describe displacements and stresses around the crack front as well as the analysis of fatigue crack propagation. Depend on the SIFs several methods were developed to calculate it using analytical, experimental and numerical techniques. Among these methods are Irwin's [21], Paris law [22], Tanaka's [23], Richard [3], and Demir's [24] model.

As the crack propagates larger, the SIF increases, until it reaches a critical range, where the assembly might start to deform by initiating fracture [19]. To prevent failure due to fatigue, extensive research has been performed to get developed and to predict fatigue crack propagation and fatigue lifetime under mixed-mode conditions. The proposed criteria for predicting the fatigue crack growth based on the value of the SIF are still being investigated. In fact, some of these criteria are appropriate for ductile materials, whereas others are appropriate for brittle materials. However, there are inconsistencies in these criteria in this regard.

Several models that have been proposed are widely employed in experiments and numerical simulations of mixed-mode fatigue crack growth but experimenting is generally expensive and time-consuming. However, from the various model developed which model is suitable to fatigue crack propagation, especially for educational and research activities, one of the problems needs to be assessed. To overcome the problem raised, this research examines which fatigue crack model of mixed-mode can better predict fatigue crack growth rate close to experimental data using extended finite element and analytical method.

1.3. Research Questions

1. What methods should be used to analyze the research problem?
2. How is fatigue crack rate investigated under mixed-mode loading conditions?
3. Which models predict fatigue life close to experimental data and how the test results are affected by different models?

1.4. Objective

1.4.1. General Objective

The main objective of this research is to conduct mixed-mode I/II fatigue crack growth rate and path prediction using analytical and numerical methods for various equivalent stress intensity factor models.

1.4.2. Specific Objectives

- ✓ To investigate mixed-mode (I/II) fatigue crack growth rate under different loading condition

- ✓ To conduct numerical simulation of the fatigue crack growth using the CTS specimen geometry using SMART crack growth simulation technology
- ✓ To evaluate the direction for further crack propagation by using maximum tangential stress (MTS) criterion
- ✓ To validate the analytical and numerical value with relevant test data from the literature

1.5. Scope of the Study

This thesis focuses on the use of the ANSYS workbench 2021 R1 in crack analysis of the engineering structures containing discontinuities and holes. This can be accomplished by using both analytical and XFEM approaches for modeling the fatigue behavior of the CTS problem. For analytic approaches, different fatigue models from previous experimental studies was used. For numerical approaches, different computational tools were used. Mainly, three approaches were commonly used in fatigue assessment of materials, i.e. (1) the fracture mechanics method, which is relatively established, (2) the strain-life method, and (3) the stress-life method. In this study, the first method will be used for fatigue crack growth rate by which the crack tip can be individually defined by the SIFs. The SMART crack growth was also be used to simulate crack growth and determine the effect of the fatigue crack path accurately to predict the fatigue life assessment. To this end, the maximum tangential stress criterion theory is used to predict the crack deflection angle. Finally, the analytical results and FE analysis were compared with the experimental and analytical data for various models.

1.6. Limitation of the Study

Methods based on fracture mechanics could be used to model and analyze the fatigue crack propagation and subsequent failure of the structure. These methods have already shown their reliability in the aerospace and automobile industry. However, the scope of this thesis is limited to the variability in the constants of the fitted fatigue crack growth models and further limited to Linear Elastic Fracture Mechanics (LEFM). While LEFM assumes small deformations and minimal yielding at the crack tip, Elastic-Plastic Fracture Mechanics (EPFM) can account for large deformations and plastic effects. And also the use of LEFM model has several advantages as it significantly reduces the need for experiments.

1.7. Motivation of the Research

Fracture has been an issue in mechanical structures for as long as man-made structures have existed. Since more can go wrong in our dynamic technological world, the problem could be worse today than in previous centuries. Without advanced aerospace technology, major airline accidents, for instance, would not be practicable [5]. The knowledge of the mechanical behavior of structures subjected to cyclic loading is a very important issue. It allows engineers to do a proper design, therefore, the relevant mechanical properties and behavior must be well known and understood; this includes mixed-mode fracture mechanics problems.

In engineering applications, sixty percent to eighty percent of structural failures are caused by cyclic loadings, and fatigue failure is a common phenomenon that has long been deliberated by researchers, engineers, and designers [12, 13], which affects the economy of one's country dramatically. Figure 1.2 shows some of the mechanical components failed due to cyclic loading. At present, there is no standardized testing method for mixed-mode crack growth. Therefore, the research on the mixed-mode fatigue crack growth behavior has no standardized conclusion. This has motivated me to examine which fatigue crack model of mixed-mode can predict fatigue crack growth rate close to experimental data.

Figure 1.2: Mechanical Components Failed Due to Fatigue Crack

CHAPTER 2 Literature Review

The overview of up-to-date theoretical, numerical, and experimental investigation in fatigue crack growth of mixed-mode I/II is presented. An overview of fatigue cracks initiation and propagation of mixed-mode I/II as well as mode I fatigue crack growth are presented.

2.1. The Fracture Mechanics Approach to Design

In general, two forms of failure in solids exist, (1) permanent (plastic) deformation and (2) breakage. The classical failure theory describes failure of a structure due to the relation between applied stress and yield or tensile strength as illustrated in Figure 2.1.

Figure 2.1: Relation of Classical failure theory

The study of the propagation of cracks in materials is the subject of fracture mechanics. Analytical solid mechanics methods are used to quantify the driving force on a crack, and experimental solid mechanics methods are used to characterize the material's fracture resistance. There are three main variables in the fracture mechanics method. Flaw size is a new structural element, and fracture hardness has replaced resilience as the most important material property. The essential variations of these three variables are quantified in fracture mechanics (Figure 2.2).

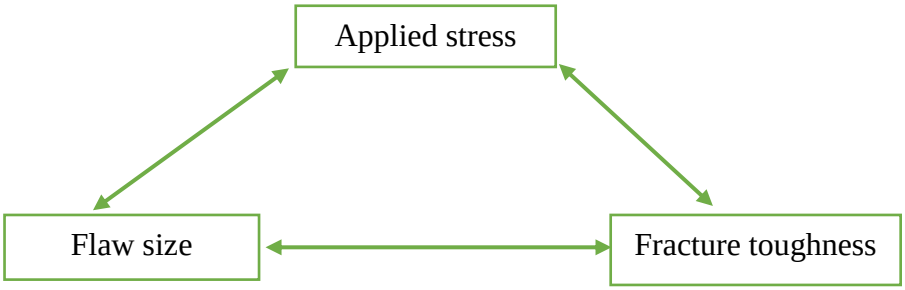

Figure 2.2: The fracture mechanics approach.

Under cyclic applied loading or a constant load in a hostile chemical environment, a crack in a component may expand. Fatigue crack growth refers to crack growth caused by cyclic loading. The analysis of faults and defects coalescence and dissemination is critical when determining the responsibility of automotive components and machinery, as well as when studying the life prediction of systems and assessing structural integrity.

Fracture mechanics is broadly divided into two types: (1) LEFM, and (2) EPFM. LEFM assumes small deformations and minimal yielding at the crack tip, while EPFM can account for large deformations and plastic effects [5]. The fracture toughness vs. stress variation is shown in Figure 2.3, for brittle materials with low toughness value, the stress variation and fracture toughness varies linearly when $\sigma < 0.8\sigma_y$, and the LEFM is taking into account. For a ductile material that obtains a higher toughness value, the LEFM approach is not adequate, and the EPFM covers this area. For materials that obtain a very high toughness value, the limit load analysis from classical failure theory must be taken into account because the high-stress level is insensitive to toughness [5]. One of the main goals in the fields of Fracture Mechanics, namely the LEFM or the EPFM, is to accurately predict the crack extension of structural components and their eventual failure (EPFM) [26].

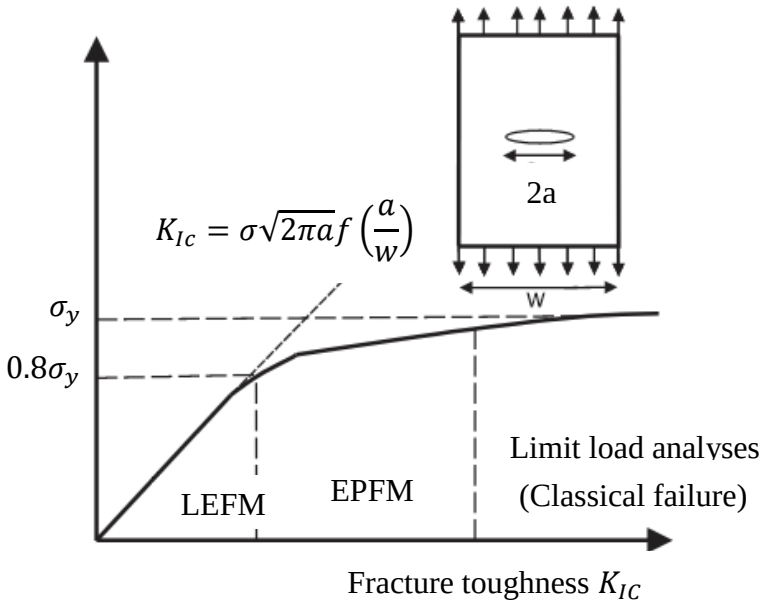

Figure 2.3: Effect of fracture toughness on the governing fracture mechanism.

In this master thesis, focus will be done on the LEFM approach to determine the crack propagation trajectories, and lifetime determination.

2.2. Griffith Energy Balance

Due to the stresses that impact the system, two new surfaces are produced during fracture, and the total energy of the system is either decreased or constant. Griffith proposes an energy balance between potential energy and the work required to form a crack. Under equilibrium conditions, an incremental increase in crack area is given by [5].

$$\frac{dE}{dA} = \frac{d\Pi}{dA} + \frac{dW_s}{dA} = 0 \tag{2.1}$$

or

$$-\frac{d\Pi}{dA} = \frac{dW_s}{dA} \tag{2.2}$$

where E is the total energy; Π the potential energy supplied by the internal strain energy and external forces; W_s is the work required to create new surfaces: and dA increase in crack area. This relation can be showed by a cracked plate, as illustrated in Figure 2.4, subjected for an increase in crack area dA due to crack increment da, and create two new surfaces.

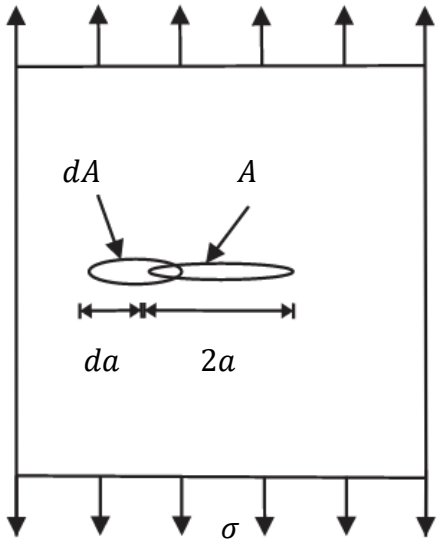

Figure 2.4: Through crack subjected for increase in crack area

For the cracked plate illustrated in Figure 2.4, Grifth used the stress analysis of Inglis to show that:

$$\Pi = \Pi_o - \frac{\pi\sigma^2 a^2 B}{E} \tag{2.3}$$

where Π_o is the potential energy of an uncracked plate and B is the plate thickness. Since the formation of a crack requires the creation of two surfaces, W_s is given by:

$$W_s = 4aB\gamma_s \tag{2.4}$$

where γ_s is the surface energy of the material and $4aB = 2\ dA$

A schematic plot of the energy variation with corresponding crack length is showed in Figure 2.5, where the total energy is expressed as:

$$E_{tot} = E_{pot} + W_s \tag{2.5}$$

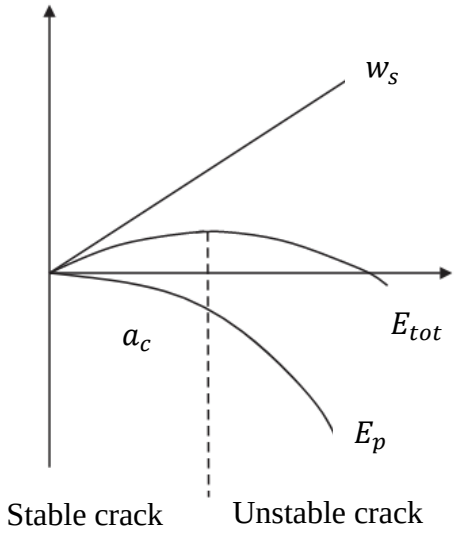

Figure 2.5: Energy variation with corresponding crack length

Similarly, a corresponding critical stress level is obtained by differentiating Equation (2.3) and Equation (2.4) with respect to increase in crack area from Equation (2.2).

$$-\frac{d\Pi}{dA} = \frac{\pi\sigma^2 a}{E} \tag{2.6}$$

and

$$\frac{dW_s}{dA} = 2\gamma_s \tag{2.7}$$

Equating Equation (2.6) and (2.7) solving for critical stress σ_c

$$\sigma_c = \sqrt{\frac{2\gamma_s E}{\pi a}} \tag{2.8}$$

The surface energy γ_s depends on material behaviour and are typical given for brittle materials, when the material become more ductile a factor γ_p, that ensure plastic behaviour, is introduced.

$$\sigma_c = \sqrt{\frac{2E(\gamma_s + \gamma_p)}{\pi a}} \tag{2.9}$$

A generalized expression for any type of energy dissipation is given by:

$$\sigma_c = \sqrt{\frac{2Ew_f}{\pi a}} \tag{2.10}$$

Where w_f is the fracture energy that include which could include plastic, viscoelastic, or viscoplastic effects, depending on the material [5], w_f describe whether or not fracture occur, due to a given value of energy release rate.

The energy release rate is compared to the fracture energy w_f required to generate two new surfaces, and a critical value of energy release rate become:

$$G_c = \frac{W_s}{dA} = 2w_f \tag{2.11}$$

And the crack propagation occur when $G \geq G_c$, this behaviour is described by the resistance curve [5].

2.3. Resistance Curve

Crack extension occurs when $G = 2w_f$; but crack growth may be stable or unstable, depending on how G and w_f vary with crack size. To illustrate stable and unstable behavior, it is convenient to replace $2w_f$ with R, the material resistance to crack extension.

The R-curve is derived from the fracture toughness data of a material. The driving force curve, which shows the change in energy release rate as a result of fracture propagation, is a corresponding curve to the R-curve. When the driving force curve exceeds the R-curve value, a fracture occurs, and the following equation is used to describe it:

$$\frac{dG}{da} \geq \frac{dR}{da} \tag{2.12}$$

The R-curve describes the behavior of a material as a result of fracture propagation. The R-curve takes on different shapes depending on the material; for ideal brittle materials, the R-curve remains constant, whereas for ductile materials, the R-curve typically rises. In Figure 2.6 two R-curves with four corresponding driving force curves ($\sigma_1 - \sigma_4$) is showed [5].

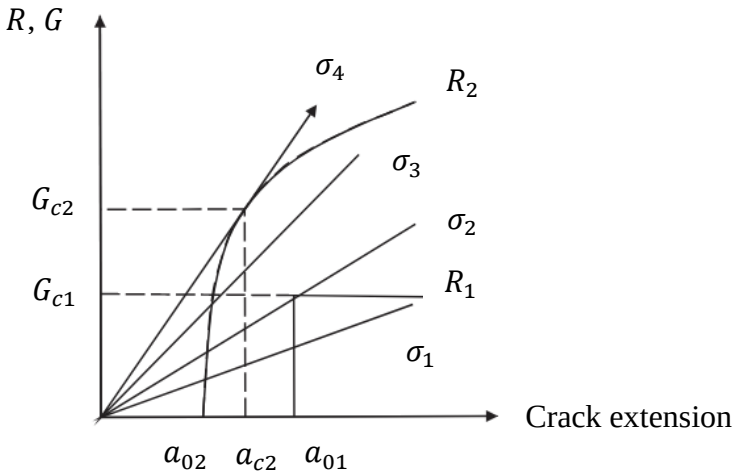

Figure 2.6: Two R-curve with corresponding four driving force curve 1-4

The first R-curve R_1 is a flat curve with a critical energy release value G_{c_1} if the driving force curve exceeds this value the crack become unstable, σ_1 is stable, no crack propagation occur and σ_2 is unstable and crack propagation occur. The second R-curve R_2 is a rising curve, where σ_3 is stable and σ_4 is unstable but opposite the constant curve the crack is allowed to propagate to a critical value a_{c_2} with a corresponding critical energy release rate G_{c_2}.

2.4. Stress Analysis of Cracks

The stress distribution around a crack-tip is schematic sketch in Figure 2.7(a). Two stress component are assumed a singular and a non-singular stress component. Where the singular part is the stresses in the vicinity of the crack-tip and the non-singular part is the stresses away from the crack-tip [5].

Griffith found a relationship between the variations of the singular stresses and the distance from the crack-tip with $1/\sqrt{r}$ singularity, when $r \to 0$ the stress is going to be infinity. Irwin developed the stress intensity factor K that describe the crack-tip conditions relative to stress, strain and

displacement near the crack tip. The stress intensity factor for each loading mode with subscript I-III are present.

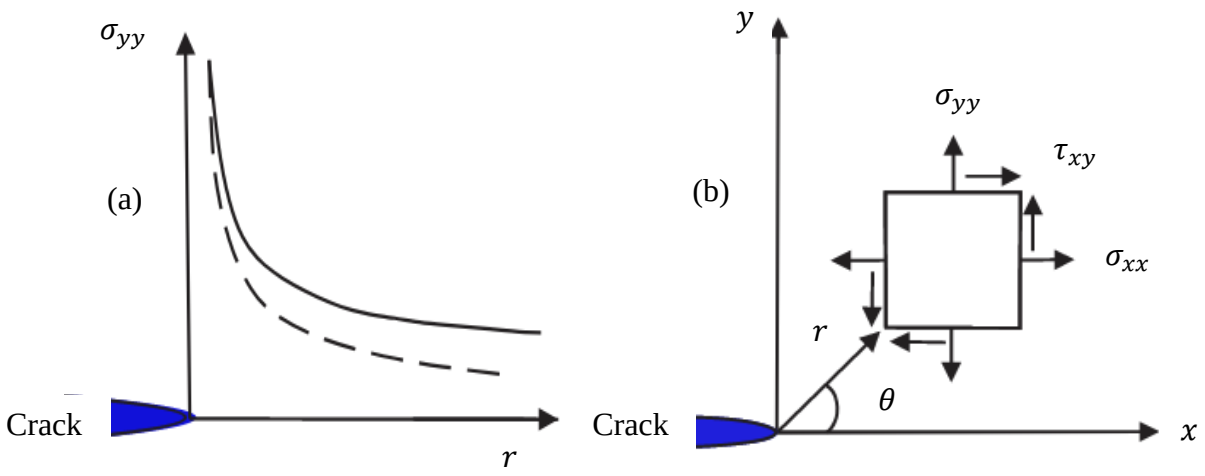

Figure 2.7: a) Stress variation around crack tip, b) Stress components in polar coordinates

From Figure 2.7(b) the coordinate system ahead of the crack-tip and the polar coordinate are defined. The singular stress fields are given as functions of the three modes of loading from the polar coordinate system r, θ [5].

$$\sigma_{xx} = \frac{K_I}{\sqrt{(2\pi r)}} cos\left(\frac{\theta}{2}\right)\left[1 - sin\left(\frac{\theta}{2}\right) sin\left(\frac{3\theta}{2}\right)\right] - \frac{K_{II}}{\sqrt{(2\pi r)}} sin\left(\frac{\theta}{2}\right)\left[2 + cos\left(\frac{\theta}{2}\right) cos\left(\frac{3\theta}{2}\right)\right] \tag{2.13}$$

$$\sigma_{yy} = \frac{K_I}{\sqrt{(2\pi r)}} cos\left(\frac{\theta}{2}\right)\left[1 + sin\left(\frac{\theta}{2}\right) sin\left(\frac{3\theta}{2}\right)\right] + \frac{K_{II}}{\sqrt{(2\pi r)}} sin\left(\frac{\theta}{2}\right)\left[2 + cos\left(\frac{\theta}{2}\right) cos\left(\frac{3\theta}{2}\right)\right] \tag{2.14}$$

$$\sigma_{xy} = \frac{K_I}{\sqrt{(2\pi r)}} cos\left(\frac{\theta}{2}\right) sin\left(\frac{\theta}{2}\right) cos\left(\frac{3\theta}{2}\right) + \frac{K_{II}}{\sqrt{(2\pi r)}} sin\left(\frac{\theta}{2}\right)\left[1 - sin\left(\frac{\theta}{2}\right) sin\left(\frac{3\theta}{2}\right)\right] \tag{2.15}$$

The stress intensity factor defines the amplitude of the crack tip singularity. That is, stresses near the crack tip increase in proportion to K. Moreover, the stress intensity factor completely defines the crack

tip conditions; if K is known, it is possible to solve for all components of stress, strain, and displacement as a function of r and θ. This single-parameter description of crack tip conditions turns out to be one of the most important concepts in fracture mechanics.

2.5. Cracks and Crack Modes

Under cyclically changing loads, cyclic fatigue causes microstructural damage and failure of materials [27]. Cracks are localized separations of a structure's substance. The force flow in the component is significantly disrupted by these material separations. The force flow is abruptly diverted, resulting in the formation of a local single stress field near the crack tip or crack front [3]. When a cyclic load is applied to a material, the stress intensity range is calculated as

$$\Delta K = Y\Delta\sigma\sqrt{\pi a} \tag{2.16}$$

A fluctuating stress intensity drives the crack to grow at some rate. When a stress intensity range ΔK is applied to a material for some number of cycles ΔN, this drives the crack to grow in length by a specific amount Δa.

As indicated in Figure 1.1, each one of the three loading modes is associated with a strain energy release rate, G_I, G_{II}, G_{III}, or the crack tip stress intensity factor, K_I, K_{II}, K_{III}, where the strain energy release rates are related with the corresponding stress intensity factor. According to Kanninen and Popelar [28], in a general way, the strain energy release rate is given by,

$$G = \frac{1}{E'}(K_I^2 + K_{II}^2) + \frac{1}{2\mu}K_{III}^2 \tag{2.17}$$

where $E' = E$ for plane stress and $E' = \frac{E}{(1-\nu^2)}$ for plain strain and μ is the shear modulus.

$$\mu = \frac{E}{2(1+\nu)} \tag{2.18}$$

If loading corresponds to mode I only, this implies that the values of K_{II} and K_{III} are equal to zero, so it can be concluded that for this situation the relation between the energy release rate and stress intensity factor is,

$$G_I = \frac{K_I^2}{E'} \tag{2.19}$$

In the case of loading of mode II only, the K_I and K_{III} are equal to zero, therefore the relation between G_{II} and K_{II} can be described by,

$$G_{II} = \frac{K_{II}^2}{E^\iota} \tag{2.20}$$

For pure mode III, the relation between the stress intensity factor and the strain energy release rate is the following,

$$G_{III} = \frac{1}{2\mu} K_{III}^2 \tag{2.21}$$

In most cases, cracks in objects or bodies are not orthogonal to longitudinal or transverse directions, i.e. they are inclined. Mixed-mode fracturing occurs when a material or body is exposed to inclined cracks and/or multiaxial stresses. When the corresponding fracture mechanics parameter, i.e., fracture hardness, approaches its critical value, the fracture is assumed to occur with a fractured body under single-mode loading. For mixed-mode fractures, though, this fracture standard can be non-conservative [10].

For the estimation of residual life and damage tolerance analysis, fracture mechanics and fatigue principles are commonly used. Mixed-mode stress fields remain at the crack tip even under mode I loading due to the complexity of the externally applied load and the random orientation of the crack [29]. The mixed-mode analysis of branched cracks requires the determinations of stress intensity factors for the original and branched crack parts in terms of the stress field surrounding the crack tip [13, 18–24]. There has been a significant amount of research done to compare the mixed-mode (I/II) FCG rate with a different stress, displacement, and energy-dependent parameters [35].

2.6. Fatigue Crack Growth Models

Many crack growth models have been developed to describe the relationship between da/dN and ΔK within the three regions of generalized crack growth behavior seen in Figure 2.8.

2.6.1. Paris Crack Growth Model

The behavior of a material under cyclic stress and the forecast of a component's service life, whether or not it has a flaw, are essential engineering topics. It is critical to predicting the fracture propagation velocity if the component has a flaw, such as a crack. Paris suggested a propagation law to better comprehend this type of problem, which is still in use today [22].

If the FCGR is plotted versus the stress intensity range in log–log scale, one can divide the crack growth into three regions, as seen in Figure 2.8 [27]. There are three distinct regions to this curve. The crack growth rate in a region I is exceedingly slow, implying that a large number of cycles are required to cause a significant change in crack size. The lower limit of ΔK, in this region, corresponds to the value of ΔK_{th} which is the minimum value for ΔK below which there is no propagation. Region II is the stable fracture propagation area; the slope of the curve in this region is almost linear when expressed in logarithmic scale, and it can be fitted by the equation established by Paris in [22]. The growth can be expressed by Paris law which is defined as

$$\frac{da}{dN} = C(\Delta K_{eq})^m \tag{2.22}$$

where C and m are the material-dependent Paris constant and Paris exponent, respectively, obtained from the mode I FCG experiments.

Finally, region III is the unstable crack propagation zone, which implies that the change in crack length over a small number of cycles will be large; the upper limit of this zone is defined by the value of ΔK_c, which corresponds to the associated material's fracture toughness.

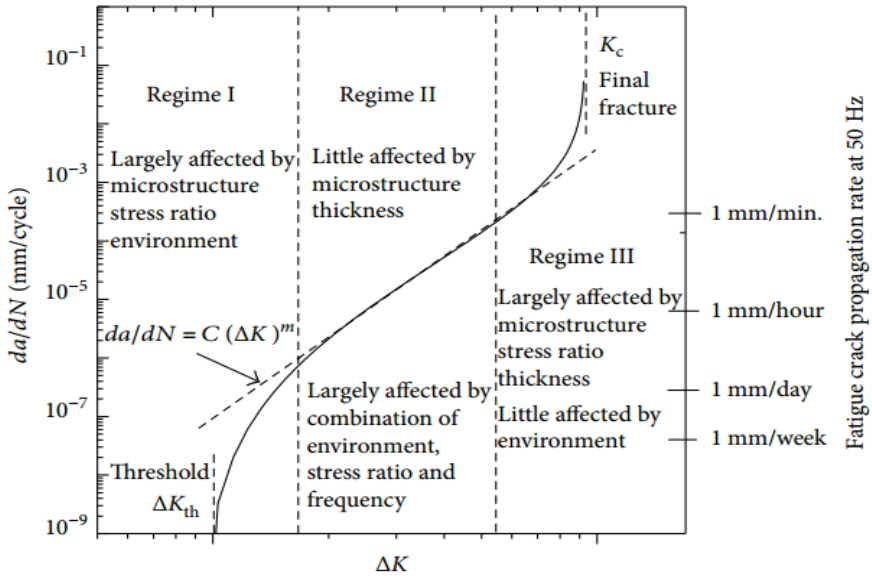

Figure 2.8: Typical crack growth curve on log-log axes.

For a given set of test conditions, stress ratio $R = \frac{\sigma_{min}}{\sigma_{max}}$, temperature and material, Paris law is describing the crack growth in the second region. Although equation coefficients can be set for a given stress ratio, the Paris–Erdogan equation does not explicitly incorporate the influence of stress ratio. Other crack development equations, such as the Forman equation and the Elber equation, explicitly incorporate the influence of stress ratio, whereas the Elber equation models the effect using fracture closure.

2.6.2. Walker Crack Growth Model

To account for the influence of stress ratio R on crack growth rate, the Walker equation is a generalization of the Paris equation. The Walker equation takes the following form [36]:

$$\frac{da}{dN} = C\left(\frac{\Delta K}{(1-R)^{1-\gamma}}\right) = C(K_{max}(1-R)^{\gamma})^{m} \tag{2.23}$$

where, γ is a material parameter which represents the influence of stress ratio on the fatigue crack growth rate. Typically, γ takes a value around 0.5, but can vary between $0.3 - 0.5$.

2.6.3. NASGRO Equation

In later years more involved models that can include all three regions and also include the influence of the stress ratio have been developed. One such equation is the NASGRO-equation used in the software with the same name. The NASGRO equation is described in the NASGRO manual [37], and is defined as

$$\frac{da}{dN} = \left[\left(\frac{1-f}{1-R}\right)\Delta K\right]^{n} \frac{\left(1-\frac{\Delta K_{th}}{\Delta K}\right)^{p}}{\left(1-\frac{K_{max}}{K_c}\right)^{q}} \tag{2.24}$$

where C, n, p and q, are the parameters of the material to be adjusted, $K_{eff} = K_{max} - K_{op}$, R is the load ratio, and K_{th} are the effective and threshold stress intensity factor ranges, respectively, and K_{max}, K_{op} and K_c are the maximum, crack opening and critical stress intensity factors, in that order. The function f is $f = K_{op}/K_{max}$.

2.7. Equivalent Stress Intensity Factors

Different procedures have been proposed to calculate the equivalent stress intensity factor, which is an important variable in order to correlate the crack behavior when a cracked structure is subjected to mixed-mode loading.

2.7.1. Irwin's Approach

Fracture standards for predicting crack initiation and propagation under mixed-mode loading have been established after extensive testing. For instance, Irwin [21] has originally developed a new concept to describe the severity of the stress distribution around the crap tip. Using the definition of Irwin, potential energy release rate G in mixed mode (I/II) loading conditions and its relation to the SIFs K_I and K_{II} under plane stress conditions, an equivalent SIF ΔK_{eq} can be derived:

$$\Delta K_{eq} = \sqrt{\Delta K_I^2 + K_{II}^2} \tag{2.25}$$

2.7.2. Paris Crack Growth Model

The theory proposed by Erdogan and Sih is called Paris law. This criterion is one of the most commonly used criteria for in-plane mixed-mode problems. Erdogan F. and Sih [22] theoretically predicted that a crack evolves perpendicularly to the maximum tangential stress at the crack tip in brittle materials under mixed-mode loading. If this tangential stress exceeds a critical value or an equivalent stress intensity factor (K_{eq}) reaches the fracture toughness (K_{IC}) value of the material, crack propagation becomes unstable, and fracture occurs. K_{eq} and the crack deflection angle for this criterion is expressed by

$$K_{eq} = cos\phi_0 \left[K_I cos^2 \frac{\phi_0}{2} - \frac{3}{2} K_{II} sin\, \phi_0 \right] = K_{IC} \tag{2.26}$$

$$\phi_0 = -arccos\left(\frac{3K_{II}^2 + K_I\sqrt{K_I^2 + 8K_{II}^2}}{K_I^2 + 9K_{II}^2} \right) \tag{2.27}$$

where K_I and K_{II} are the SIFs of mode-I and mode-II, respectively; ϕ_0 is the crack deflection angle.

2.7.3. Tanaka's Models

Tanaka [23] proposed a modified form of the Paris law to correlate the fatigue crack growth rate $da = dN$ with the mixed-mode SIFs. The equivalent stress intensity factor ΔK_{eq} is given by:

$$\Delta K_{eq} = (\Delta K_I^4 + 8\Delta K_{II}^4)^{1/4} \quad (2.28)$$

2.7.4. Richard Criterion

Richard et al. [38] developed an empirical fracture criterion, which built a relationship between all three modes of fracture and Mode I fracture toughness to simplify the prediction of crack growth under multiaxial loading. This criterion was later modified by Richard et al. [34] to fit the testing results of different brittle materials. The equivalent SIF and crack deflection by the following equation:

$$K_{eq} = \frac{K_I}{2} + \frac{1}{2}\sqrt{K_I^2 + 4(\alpha_1 K_{II}^2)} \leq K_{IC} \quad (2.29)$$

where α_1 is a material parameter describing the ratio of K_{IC}/K_{IIC} and generally taken as 1.155.

2.7.5. Demir's Model

Recently, Demir et al. [24] proposed another model for ΔK_{eq} using the nonlinear regression analysis of the numerical and experimental results of the CTS specimen. This model is proposed for use at higher load mixity levels. The model is verified using a T-type mixed-mode specimen. Their model is given by:

$$\Delta K_{eq} = (1.0519\Delta K_I^4 - 0.035\Delta K_{II}^4 + 2.3056\Delta K_I^2 \Delta K_{II}^2)^{1/4} \quad (2.30)$$

A summary of many currently available models can be found in reference [21-25].

2.8. Prediction of Fatigue Crack Direction.

During crack growth under mixed-mode loading, crack growth direction changes per mode mixity ratio. Thus, for accurate assessment of life predictions, crack growth direction plays a key role along with the fatigue crack growth rate under mixed-mode loading conditions.

It is well known that the crack propagation phenomenon is highly dependent on the state of stress in the vicinity of the crack tip, therefore, SIF is considered as the most significant parameter in predicting the crack propagation path.

2.8.1. The Maximum Energy Release Rate Criterion

In the group of energy-based criteria, the maximum energy release rate, MERR criterion predicts that the crack will initiate along the direction where the energy release rate reaches the maximum [31].

However, as it is difficult to obtain an analytical solution to the energy release rate in an arbitrary direction for a cracked body, the application of the MERR criterion is very limited [8, 23].

2.8.2. Minimum Strain Energy Density Criterion

The minimum strain energy density SED-criterion [32] states that the direction of crack initiation coincides with the direction of minimum strain energy density along a constant radius around the crack tip. The strain energy density of a near crack tip element is expressed as follows

$$S = a_{11}K_I^2 + 2a_{12}K_IK_{II} + a_{22}K_{II}^2 + a_{33}K_{III}^2 \tag{2.31}$$

where K_{III} is the mode-III SIF ($K_{III} = 0$) and a_{11}, a_{12}, a_{22}, and a_{33} can be obtained as follows:

$$a_{11} = \frac{1}{16\pi\mu}(3 - 4v - cos\theta)(1 + cos\theta) \tag{2.32}$$

$$a_{12} = \frac{1}{8\pi\mu}(cos\theta - 1 + 2v)sin\theta \tag{2.33}$$

$$a_{22} = \frac{1}{16\pi\mu}[4(1 - v)(1 - cos\theta) + (1 + cos)(3cos\theta - 1)] \tag{2.34}$$

$$a_{33} = \frac{1}{4\pi\mu} \tag{2.35}$$

where μ is the shear modulus and v is Poisson's ratio. The initiation angle (θ_0) can be obtained by

$$\frac{\partial S}{\partial \theta} = 0, \frac{\partial^2 S}{\partial \theta^2} > 0$$

This new strain energy density factor has a simple mathematical expression. It is also able to handle various combined loadings. However, this 3D MSED criterion was found to be inconsistent with some experimental results in Mageed and Pandey [25, 26].

2.8.3. Maximum Tangential Stress

The maximum tangential stress MTS-criterion [22] is the simplest criterion and it states that the direction of crack initiation coincides with the direction of the maximum tangential stress along a constant radius around the crack tip. The equivalent mode-I stress intensity factor (K_{Ie}), which is transformed from the mixed mode I-II fracture, is defined as follows:

$$K_{Ie} = \frac{1}{2}\cos\frac{\theta_0}{2}[K_I(1 + cos\theta_0) - 3K_{II}\sin\theta_0] \tag{2.36}$$

where the initiation angle, θ_0

$$\theta_0 = 2\arctan\frac{1-\sqrt{1+8(K_I/K_{II})^2}}{4K_{II}/K_I} \tag{2.37}$$

When K_{Ie} equals the mode-I fracture toughness (K_{IC}), the crack initiates, and K_I is 0 for a closed crack.

When $\frac{K_{II}}{K_I} \to \infty$,

$$\lim_{\frac{K_{II}}{K_I}\to\infty} \frac{1-\sqrt{1+8\left(\frac{K_I}{K_{II}}\right)^2}}{\frac{4K_{II}}{K_I}} = \frac{1}{\sqrt{2}} \tag{2.38}$$

Thus, $\theta_0 = 70.5°$ and K_{Ie} becomes maximum for closed cracks.

In stress-based criteria, the (MTS) criterion has become one of the most commonly used criteria due to its simplicity and good agreement with the micromechanical models [45]. This maximum tangential stress criterion proposed by Erdogan and Sih [18] is widely in use for mixed-mode (I/II) crack path prediction and is employed in the present numerical studies.

2.9. Finite Element Methods to Simulate Fatigue Crack Growth Problems

The finite element method has its beginnings in the 1950s, and with the widespread use of the digital computer has since gained considerable favor relative to other numerical approaches. The FEM may be viewed as an approximate Ritz method combined with a variational principle applied to continuum mechanics. It permits the prediction of stress in an engineering structure, with unprecedented ease and precision. The first challenge in utilizing the finite element approach to estimate fatigue crack propagation rates is calculating sufficiently precise values for the crack's stress intensity factor at maximum and minimum applied loads throughout each cycle [17]. The stress and displacement fields of the entire component are also required to compute the stress intensity factor. Chan, et al. [46] provided three simple techniques for calculating the stress intensity factors of mode I fractures using a finite element stress field in 1970. The stress method, displacement method, and line integral method were all computed using simple linear (constant-strain) triangle elements with a high degree of refinement at the crack tip. Byskov [47] created a triangular crack tip element including required form functions to correctly represent the stress singularity in 1970 in an effort to solve difficulties with

modeling the stress singularity. In 1973, Wilson [48] extended this method to circular elements, and in 1974, Hardy [49] extended it to rectangular elements. Holston [50] created a mixed-mode version of the circular element in 1976, and Jiang and Cheung [51] developed a bending-specific version in 1995.

Stress and strain analysis, wave propagation, heat transfer, electrical and magnetic fields, and fluid flow are some of the issues that the FEM has been used to solve. Currently, commercial programs like as Abaqus, ANSYS, and Zencrack software provide finite element analysis software. For fracture mechanics, XFEM is used to keep these codes up to date.

2.9.1. The J-integral

The J-integral is a mathematical notion that allows you to compute an energy release rate even when plasticity cannot be neglected. This integral is path independent, allowing the same result to be obtained for various contour integral pathways. The initial form of the integral is given by J. Eshelby in [52], and it is based on the theorem of energy conservation, Broek in [53], defines it as:

$$J = \int_{\tau} \left(W dy - T \frac{\delta u}{\delta x} ds \right) \tag{2.39}$$

where W is the strain energy per volume unit, T is the traction tension vector, τ is the contour of the integral, u is the displacement and ds is an element of the contour τ. Figure 2.9 shows the contour around a crack, as the integral solution is path independent that means that the value of integral resulting from the path τ is the same as the result of the integral for the path τ_t.

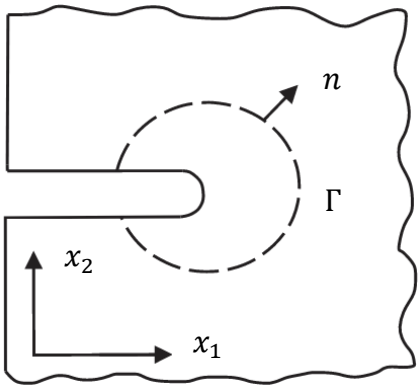

Figure 2.9: Contour around a crack.

Since the basis of the equation (2.39) is an energy conservation theorem, the J-integral is an energy related quantity. In 1968 Rice [54], has shown that the result of the J-integral is equal to the change of the potential energy around the crack tip resulting of a virtual crack extension da; the resulting equation is mentioned by Broek in [53], and has the following form:

$$J = -\frac{\delta V}{\delta a} \tag{2.40}$$

where V is the potential energy. In linear elastic cases the result of the integral is equal to energy release rate,

$$J = -\frac{\delta V}{\delta a} = G \tag{2.41}$$

For mixed mode I+II loading with small-scale yielding, the following relationship exists between the energy release rate and the stress intensity factors [14]:

$$J = G = \frac{1}{E^*}(K_I^2 + K_{II}^2) \tag{2.42}$$

where:

$$E^* = \begin{cases} E, & \text{Plane stress} \\ \dfrac{E}{1-\nu^2}, & \text{Plane strain} \end{cases} \tag{2.43}$$

E is the elastic modulus, while ν is Poisson's ratio.

2.9.2. Virtual Crack Closure Technique

The modified crack closure integral was developed by Rybicki and Kanninen [55] in 1977, based on Irwin's 1957 claim that the energy required to grow a crack is equal to the work required to close a crack of the same length. Nowadays, Rybicki and Kanninen's method is known as the VCCT.

Virtual crack closure technique is widely used for computing energy release rates based on results from 2D and 3D finite element analyses to supply the mode separation required when using the mixed-mode fracture criterion which uses the principles of linear elastic fracture mechanics.

2.9.3. Extended Finite Element Method

The crack must be included into the geometry in order for elements to align with the crack boundary in the finite element approaches mentioned thus far. Belytschko and Black [15] developed the XFEM in 1999 as a mechanism for defining fractures randomly within the mesh.

Jianxu Shi et al. [56] was incorporated XFEM into an Abaqus user defined subroutine to evaluate cyclic fracture development in standard and modified compact specimens, as well as a complicated helicopter component, in 2010. As shown in Figure 2.10 [17], XFEM models the crack (or other discontinuities) using a non-conforming mesh, i.e. the cracks are simulated independently of the mesh [14]. This is accomplished by "enriching" the elements sliced by the crack by adding special shape functions to account for local discontinuities and singularities [57].

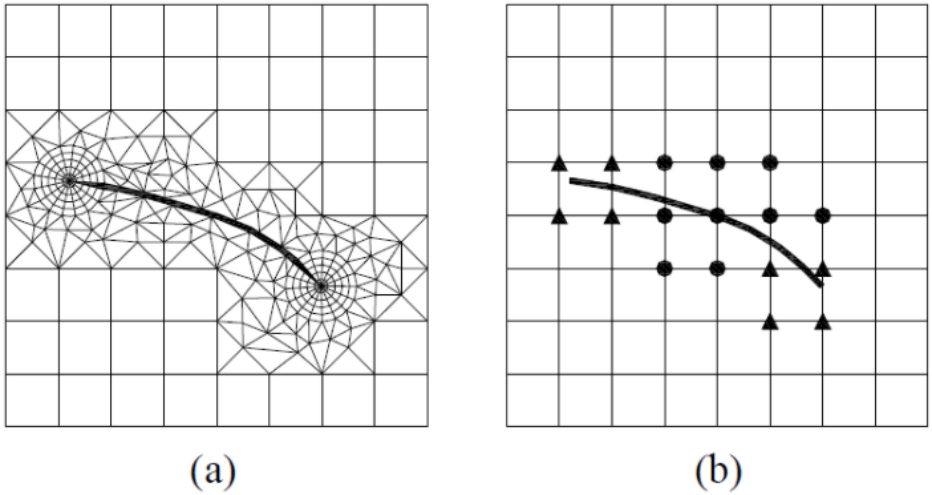

Figure 2.10: Illustrative sketches of (a) a conforming FEM mesh and (b) a nonconforming XFEM mesh.

2.10. Research Gap

A thorough review of published works of literature identified that numerous models have been proposed and developed for analyzing fatigue crack growth path behavior for different mode loading types. Among the available laws, the modified form of the Paris law proposed by Tanaka in 1974 [23] is widely used for correlating the experimental mixed-mode (I/II) FCG and for the numerical prediction of crack growth behavior. However, it is insufficient to provide definitive information about the performance of the ΔK_{eq} models for mixed-mode I/II. For mode I crack growth, most of the

fracture criteria yield similar results and agree with the test results but for pure mode II or I-II mixed mode plane fracture, the results obtained by different fracture criteria are quite different. In addition, from the various model developed which model is suitable to fatigue crack propagation, especially for educational and research activities, the problems needs to be assessed. How to choose the appropriate fracture criterion is also one of the research gaps need to be assessed, since, up to date, there is no standardized testing method for total fracture toughness of metals under mixed-mode loading.

2.11. Solution Proposed

In view of the above observed gap, in this thesis, finite element fatigue crack growth simulations will be carried out, and the effect of the ΔK_{eq} model in fatigue life prediction will be studied. The performance and capability of various models will be evaluated by comparing the predicted life with the experimental result from the literature. And based on the overall consistent performance, to predict which model is predicting life close to the experimental data for prediction of mixed mode I/II fatigue life.

CHAPTER 3 Methodology

3.1. Material, Loading and Specimen Specifications

The 7075-T651 aluminum alloy is a high-strength aluminum alloy that is primarily used in aerospace structural components, such as the CP-140 Aurora maritime patrol aircraft and the CC-130 Hercules transport aircraft operated by the Canadian Air Force [58].

The material used in this research was aluminum Al 7075-T651 alloy in the form of rolled sheets with a thickness of $5\ mm$. The mechanical properties of the alloy is given in Table 1. The fracture toughness (K_{IC}) and threshold stress intensity factor range (ΔK_{th}) of this alloy are $32.95\ MPa\sqrt{m}$ and $3.15\ MPa\sqrt{m}$ respectively.

Table 1: Mechanical properties of Al 7075-T651

Material	Yield stress	Ultimate strength	Elastic Modulus	Poison's ratio	Elongation break
Al 7075-T651	$517\ MPa$	579	$74\ GPa$	0.33	7.9%

Compact Tension Shear, CTS specimen, which was first introduced by Richard and Benitz [59], was used in the test by loading the material at various mode ratios. Figure 3.1 illustrates geometry of the CTS specimen employed in this thesis which is widely employed for the mixed mode (I/II) FCG studies.

Demir [24] carried out in-plane fatigue crack growth simulation and experiments for Al 7075-T651 aluminum alloy under different mode mixity ratios to evaluate the applicability of a fracture criterion developed in a previous study to mixed-mode-I/II fatigue crack growth tests. Fatigue crack growth experiments were performed by using Compact Tension (CT) specimens under pure mode-I loading and by using CTS specimens under in-plane mixed-mode loading. In-plane mixed-mode-I/II fracture experiments were performed under different loading angles using pre-cracked CTS specimens.

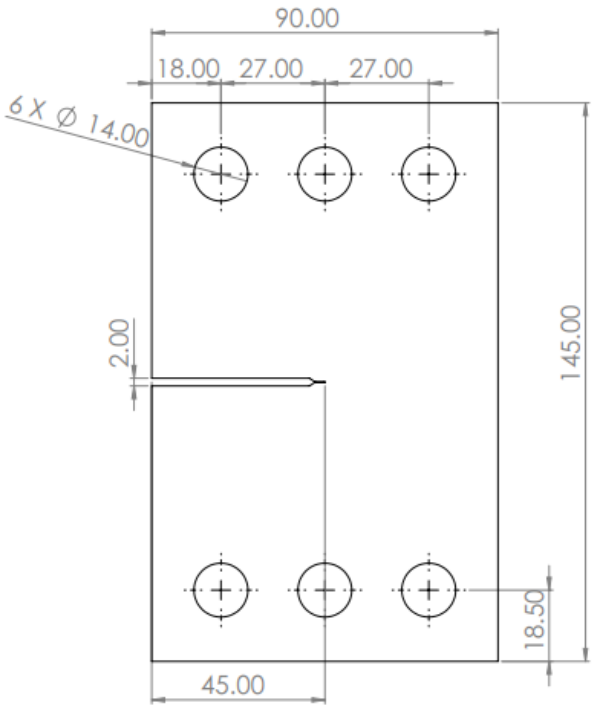

Figure 3.1: Dimensions of a CTS specimen.

Fatigue pre-cracking is carried out utilizing an axial fatigue test machine under mode-I stress according to the ASTM E647-13a standard before fatigue crack growth tests. The number of cycles is recorded simultaneously while crack propagation is observed and controlled using a high-zoom camera and split sub-millimetric scales on specimens. All fatigue crack growth tests are done at $R = 0.1$ (where R is the stress ratio) after the pre-crack is generated. SIF ranges are computed for each mode-I test based on test load ranges and updated crack lengths based on crack growth increment data. The material's fatigue fracture growth rate data is shown, and the following material constants C and m are calculated by fitting the curves.

- C = 4.3378×10^{-7} $(mm/cycle)/MPa\sqrt{m})^m$
- m = 2.6183.

3.2. Methods of Fracture Analysis

Methods based on fracture mechanics could be used to model and analyze the fatigue crack propagation and subsequent failure of the structure. These methods have already shown their reliability in the aerospace and automobile industry. The use of the LEFM model has several

advantages as it significantly reduces the requirement of experiments. Furthermore, this method can predict the crack propagation until subsequent failure, which implies that the total fatigue life of the structure can be predicted for a certain crack length. A fracture analysis typically starts with an initial crack size, or crack initiation criteria based on stress or strain, and propagates the crack until a critical value is reached such as K_c or G_c. Growth rates are calculated using various fatigue cracks growth models such as the Paris model, Richard, Demir, and other criteria select from the literature. Analytical and finite element methods will be used to provide approximate solutions.

3.2.1. Extended Finite Element Methods

Fracture simulation has relied on two models: (1) traditional cohesive zone modeling (CZM) and (2) XFEM [20], which is more recently employed. CZM is mostly used to simulate debonding between two adhesively connected surfaces. When a load is applied, delamination occurs, but the delaminating fracture is limited to the interface between the two surfaces. CZM is useful for modeling composites, however it is not ideal for modelling a fracture spreading through a material's bulk. Internal crack calculations are improved using XFEM, which was introduced a few years ago into the ANSYS SMART crack growth, and it reduces preprocessing time by employing UMM's automatically generated all-tetrahedral (tet) mesh for crack fronts.

In order to implement the determination of stress intensity factors due to crack propagation, the numerical finite element program ANSYS Workbench 2021 R1 is used. The modeling approach followed is described in Figure 3.2. The first tab of the plug-in is Model definition, and this is where the user needs to define the geometry, pre-crack length, and the loading angles. Modeling and the whole assembly of the CTS specimen is performed by SolidWorks 2021 and it is saved in IGES format to import into ANSYS workbench and then imported into ANSYS workbench. Next, the user has to input the material properties using the Material submenu. In the Engineering Data tab allows access to the material definition but in the Engineering Data tab of ANSYS workbench 2021 the properties of Al7075-T651 is not defined which is used in this thesis. Therefore, for this thesis the properties of Al7075-T651 is defined in the Engineering Data tab and assigned. After importing the geometry and assigning material, a mesh method needs to be added and set to 'Tetrahedrons'; by default the Patch Conforming algorithm will be chosen.

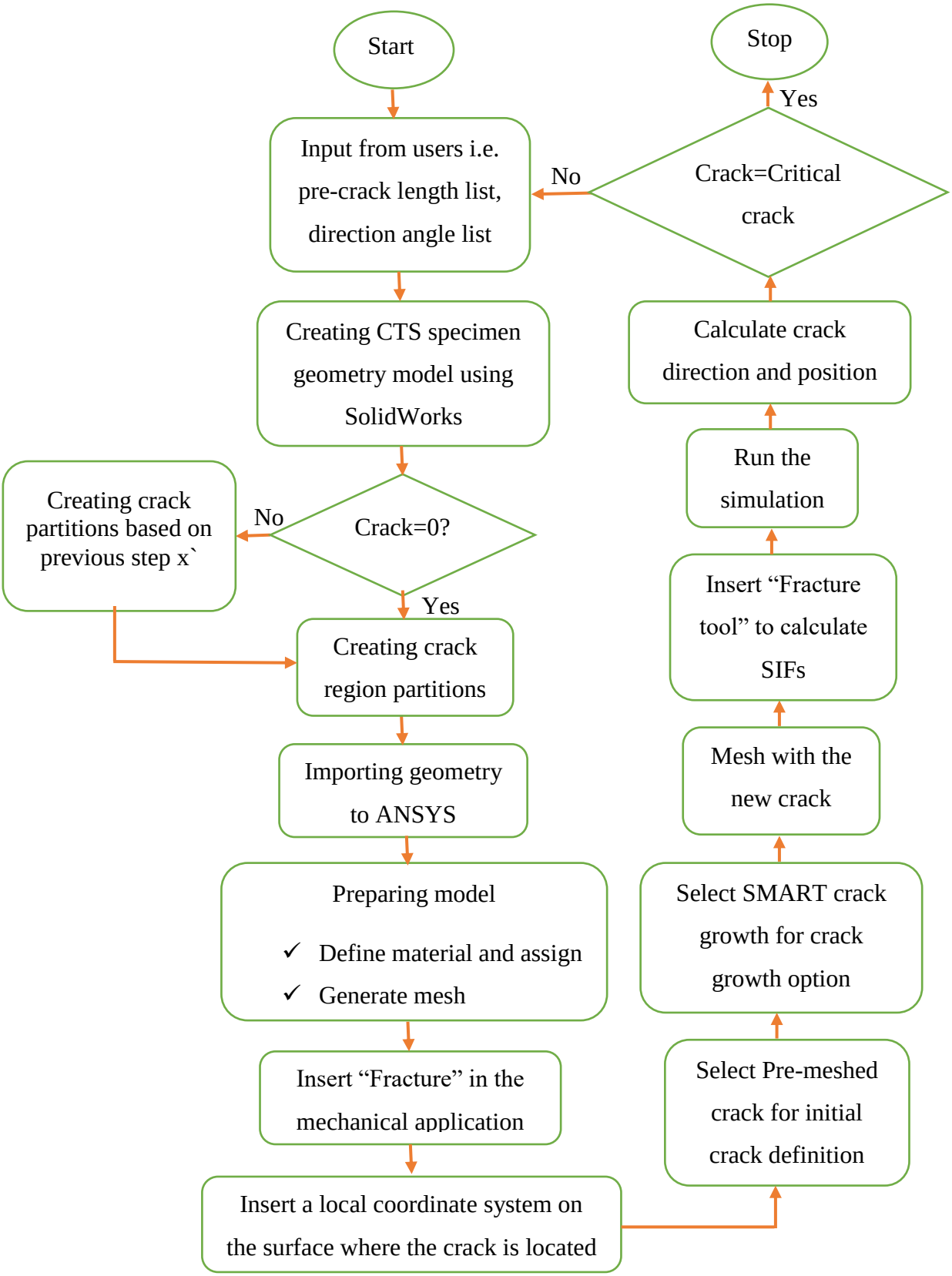

Figure 3.2: Flowchart of the script for fatigue fracture analysis of CTS specimen

The mesh size needs to be refined around the crack tip. Sphere of influence method based around the geometric edge running through thickness is chosen. To define the crack tip three named geometric regions is selected. These are (1) crack edge, (2) top surface of the crack and (3) bottom surface of the crack. Each of these regions is then associated with a node set for use in the analysis for all loading angles. A local coordinate system is defined for the crack tip. As shown in Figure 3.3, the components indicate crack propagation direction (x) and crack opening direction (y).

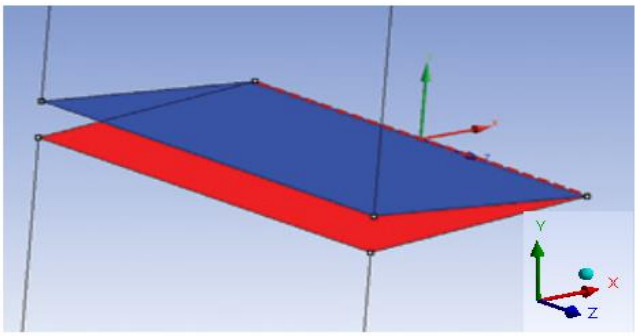

Figure 3.3: Local Coordinate System

The next step is Insert "Fracture" in the mechanical application. From the Command ribbon, the option for Fracture is chosen. Further options for introducing a crack are: Arbitrary Crack; Semi Elliptical Crack and Pre-Meshed Crack. The Pre-Meshed crack object is selected to carry out initial crack definition and within the Pre-Mesh Crack object, the Node sets created previously are allocated to the crack front, and the crack top and bottom faces. The crack coordinate system is referenced.

In the Fatigue menu ribbon, three methods are available to model the crack front and its growth: (1) Interface Delamination, (2) Contact Debonding and (3) SMART Crack Growth. SMART Crack Growth is selected, then, the SMART crack growth in ANSYS will be used to simulate crack growth and determine the effect of the fatigue crack path accurately to predict the FCG behavior.

3.2.2. Analytical Methods

The SIFs K_I and K_{II} for all the analytical conditions will then be calculated from numerical simulation of the CTS specimen under mixed-mode fatigue loading. Integrating a fatigue crack growth law such as Tanaka's model, Irwin, Demir and, Richard criterion is the most basic approach explored in this thesis for solving the fatigue fracture life of a specimen. The integral approach assumes self-similar mixed-mode crack propagation and will be used as a validation tool in this thesis.

3.3. Fatigue Crack Growth Models

Besides static loading, crack growth can occur when a subcritical load is repetitively applied. The commonly used fatigue crack growth rate equations of the type by Paris and Erdogan [22]. As illustrated in Figure 2.8, the crack growth curve can be divided into three regions of generalized behavior.

1. In the threshold region, crack growth is slow as ΔK asymptotically approaches the threshold value, ΔK_{th} where crack growth may not occur.
2. The slope of the crack growth curve is approximately linear in the intermediate, or Paris, region, and
3. The unstable region is characterized by rapid, unstable crack growth where K_{max} asymptotically approaches K_c and fracture is imminent.

Numerous crack growth models have been developed to describe the relationship between da/dN and ΔK within these regions. Among those, a few of them will be presented in this thesis.

3.4. Determination of Mixed-mode SIFs

The calculation of SIF is of great significance for the research of mixed-mode FCG due to SIF based on linear elastic fracture mechanics is the driving force of FCG. However, there is no unified solution method for the SIF of I-II mixed mode FCG process at present. The most widely accepted expression of I-II mixed mode SIF was proposed by Richard [60] based on the CTS system [9], [18]. The stress intensity factors K_I and K_{II} for the CTS specimen can be computed in the range $0.5 \leq a/w \leq 0.7$ by the following equation [60].

$$K_I = \frac{F}{wt}\sqrt{\pi a}\frac{\cos\alpha}{1-a/w}\sqrt{\frac{0.26+2.65\left(\frac{a}{w-a}\right)}{1+0.55\left(\frac{a}{w-a}\right)-0.08(\frac{a}{w-a})^2}} \quad 3.1$$

$$K_{II} = \frac{F}{wt}\sqrt{\pi a}\frac{\sin\alpha}{1-a/w}\sqrt{\frac{-0.23+1.40\left(\frac{a}{w-a}\right)}{1+0.67\left(\frac{a}{w-a}\right)+2.08(\frac{a}{w-a})^2}} \quad 3.2$$

where F is the uniaxial force applied to the loading device, a is the crack length (starter notch depth $+$ fatigue crack), w is the specimen width, t the specimen thickness, and α is mixed-mode loading

angle. However, when fatigue cracks are subjected to mixed-mode stress, they do not propagate in the same direction as they did before [61]. Furthermore, these relationships were calculated using a two-dimensional issue and do not take into account the crack front's thumbnail form. As a result, when the fracture has grown, Richard's relations cannot be used. In order to obtain the actual values of the SIFs, a numerical analysis was done for this purpose.

The extended finite element approach was used to construct a 3D simulation for different fracture geometries. The SIFs K_I and K_{II} for all the analytical conditions were then calculated from numerical simulation of the CTS specimen under mixed-mode fatigue loading. The equivalent stress intensity factor K_{eq} has been introduced for considering mode I and mode II simultaneously. Figure 3.4 shows the loading and boundary conditions used in ANSYS analysis of the present work. The bottom end holes are constrained in x and y directions. The amount of applied load is decomposed into punctual loads F_1, F_2, and F_3 and applied at the respective holes near the top end of the CTS specimen, as shown in Figure 3.4. The distribution of the loads F_1 to F_6 onto the specimen due to the applied load F is given as in [60].

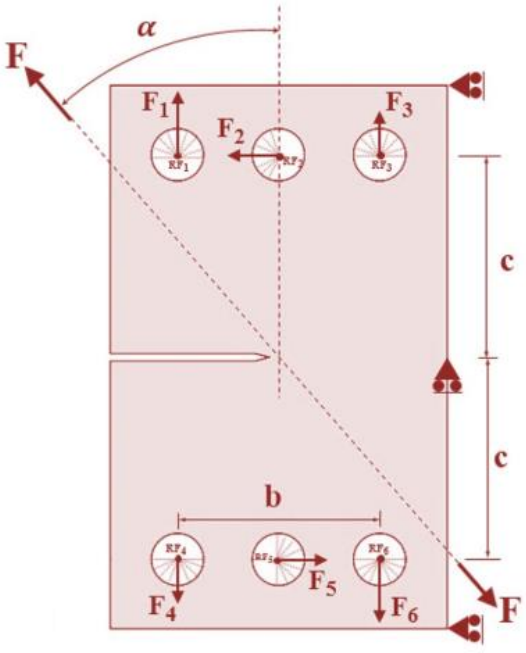

Figure 3.4: Loading and boundary condition for CTS geometry.

The uniaxial load F is correlated to the equivalent loads acting on different holes of the six holes based on the following formulas [59]:

$$F_1 = F_6 = F(0.5\cos\alpha + \frac{c}{b}\sin\alpha) \quad 3.3$$

$$F_2 = F_5 = F\sin\alpha \quad 3.4$$

$$F_3 = F_4 = F(0.5\cos\alpha - \frac{c}{b}\sin\alpha) \quad 3.5$$

where α is the angle of load and c and b are length parameters shown in Figure 3.4 (where $c = b = 54\ mm$). Note that the angle must be used in radians. The final values of all loading forces with different loading angles ($30°, 45°, and\ 60°$) are shown in Table 2.

Table 2: Values of forces F_1 to F_6 according to load angle α

α	$F_1 = F_6$	$F_2 = F_5$	$F_3 = F_4$
30°	$0.933F$	$0.5F$	$-0.067F$
45°	$1.061F$	$0.707F$	$-0.354F$
60°	$1.116F$	$0.866F$	$-0.616F$

The predicted values of ΔK_{eq} were compared to the experimental values performed by Demir [24] as well as the analytical expression given by Irwin [21], Tanaka [23], Richard [34], and Demir model [24] for different values of loading angles $30°, 45°$ and $60°$. The analytical value of SIFs with load angle of $30°$ and the amount of applied loading is $8.8\ kN$, for the loading angle of $45°$ and the amount of the load is $11.4\ kN$ and for $60°$ loading angle and the amount of load is $13.65\ kN$.

3.5. Fatigue Life Prediction

Mainly, three approaches have been commonly used for illustration of the fatigue assessment of materials which are: (1) fracture mechanics, (2) strain-life and (3) stress life method. In this thesis, the first method was used for fatigue life prediction by which the crack tip can be individually defined by the SIFs.

A 3D simulation for crack geometries was performed by the finite element method. The SIFs K_I and K_{II} for all the analytical conditions were then calculated from numerical simulation of the CTS specimen under mixed-mode fatigue loading. Different procedures have been proposed to calculate

the equivalent stress intensity factor, which is an important variable in order to correlate the crack behavior when a cracked structure is subjected to mixed-mode loading. In this thesis, four criteria's are selected from the literature (see Table 3) to calculate equivalent stress intensity factor for mixed-mode.

Table 3: Equations to calculate equivalent stress intensity K_{eq} in this thesis.

Criterion to calculate equivalent stress intensity K_{eq}	Reference
$K_{eq} = \sqrt{\Delta K_I^2 + K_{II}^2}$	Irwin [21]
$K_{eq} = (\Delta K_I^4 + 8\Delta K_{II}^4)^{1/4}$	Tanaka [23]
$K_{eq} = \frac{K_I}{2} + \frac{1}{2}\sqrt{K_I^2 + 4(\alpha_1 K_{II}^2)}$	Richard [34]
$K_{eq} = (1.0519\Delta K_I^4 - 0.035\Delta K_{II}^4 + 2.3056\Delta K_I^2 \Delta K_{II}^2)^{1/4}$	Demir [24]

The calculation of fatigue crack growth using the corresponding stress intensity factor is the most widely used method for structures under mixed-mode dynamic loading. Using a modified formula of Paris law, a researcher [22] proposed a power law for the fatigue crack growth relationship with, which is specified as in Equation (2.22).

$$\frac{da}{dN} = C(\Delta K_{eq})^m$$

From this equation, for a crack increment, the number of life cycles of fatigue may be predicted as

$$\int_0^{\Delta a} \frac{da}{C(K_{eq})^m} = \int_0^{\Delta N} dN = \Delta N \qquad 3.6$$

Several of the commonly used K_{eq} formulas accompanied by the proposed authors are listed in Table 3. Finally, percentage relative error in predicted K_{eq} (with respect to the experimental K_{eq}) for each of the four models for all three loading angles considered in this study are estimated using the following equation.

$$\text{Percentage relative error} = \frac{\text{Experimental } K_{eq} - \text{Predicted } K_{eq}}{\text{Experimental } K_{eq}} \times 100\% \qquad 3.7$$

3.6. Crack Growth Direction

For accurate assessment of life prediction, crack growth direction plays a key role along with the fatigue crack growth rate under mixed-mode loading conditions. Therefore, the fatigue crack growth direction must be precisely calculated for the evaluation of fatigue life. Under mixed-mode loading, there are several criteria for predicting crack growth direction. MERR, SED, and MTS criterion are some of the most common methods for the prediction of crack growth direction. The MTS criterion proposed by Erdogan and Sih [22] is widely in use for mixed mode (I/II) crack path prediction, and is employed in this thesis. According to this criterion, the crack propagates in a radial direction (θ_c) from the crack tip in which the tangential stress becomes maximum ($\sigma_{\theta,max}$), and as soon as $\sigma_{\theta,max}$ exceeds the material limiting value $\sigma_{\theta,c}$ unstable fracture takes place [62]. The crack deflection angle θ_c can be obtained by maximizing the tangential stress component ($\partial\sigma_{\theta,max}/\partial\theta = 0$),

$$K_I \, sin\theta_c + K_{II}(3 \, cos\theta_c - 1) = 0 \tag{3.8}$$

The solution of the above equation can be expressed as [43]

$$\theta_c = 2 \, tan^{-1}\left[\frac{1}{4}\frac{K_I}{K_{II}} - \frac{1}{4}\sqrt{\left(\frac{K_I}{K_{II}}\right)^2 + 8}\,\right] \quad \text{for} \quad K_{II} > 0 \tag{3.9}$$

$$\theta_c = 2 \, tan^{-1}\left[\frac{1}{4}\frac{K_I}{K_{II}} + \frac{1}{4}\sqrt{\left(\frac{K_I}{K_{II}}\right)^2 + 8}\,\right] \quad \text{for} \quad K_{II} < 0 \tag{3.10}$$

where positive θ_c is defined as an angle measured in the anticlockwise direction with respect to the initial crack orientation direction. Figure 3.5 (a) and (b) indicate the change in the direction of the crack growth with the sign (direction) of K_{II}.

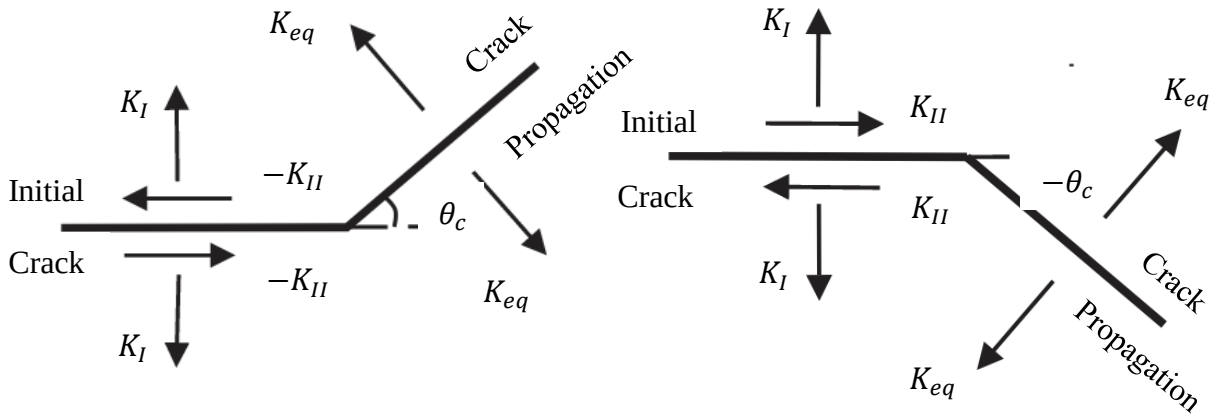

Figure 3.5: The direction of K_{II} and crack growth angle (a) positive θ_c (b) negative θ_c.

CHAPTER 4 Numerical Simulation

In order to implement the determination of stress intensity factors due to crack propagation, the numerical finite element program ANSYS Workbench 2021 R1 was used. In this section, finite element models, boundary conditions and loads are described.

4.1. ANSYS SMART Crack Growth with Unstructured Mesh Method

The "Separating Morphing and Adaptive Remeshing Technology (SMART) crack growth" function of ANSYS Workbench (version 2021 R1, ANSYS, Inc., Canonsburg, PA, USA) was used in this thesis. By using this feature in ANSYS Workbench, engineers have recently employed the modern unstructured mesh method (UMM) to minimize pre-processing times by using the automatically generated all-tetrahedral mesh for the crack fronts and achieve the same high-fidelity results as a simulation with the ideal hex mesh configuration. Meshing time has been reduced from a few days to a few minutes. With several clicks, a SMART simulation can be set up, eliminating long preprocessing sessions. UMM is more flexible and simpler to use than any previous technology for fracture simulation. Automatic remeshing is automatically done in the vicinity of the crack tip as well as refines calculations in the most needed regions with higher stresses for better visualization and accurate results calculation without requiring the engineer's intervention.

Another feature for the "SMART Crack Growth" is the introducing of the "premeshed crack." The mesh around the crack tip should be refined using the sphere of influence method around the geometric edge going through thickness (See Figure 4.1). Within the premesh crack object, the node sets created previously are allocated to the crack front and the crack top and bottom faces. There are "loops" through the mesh around the crack point that are used by the integration of the crack tip region with the strain energy to determine the stress factor. The fracture mechanics method avoids the stress singularities at the crack tip in the analysis.

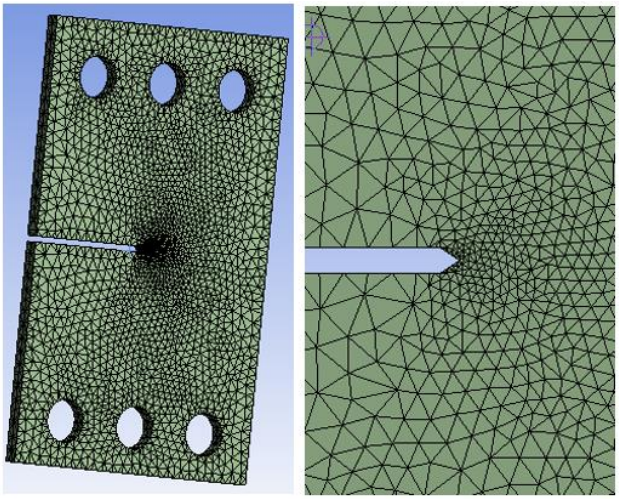

Figure 4.1: a) Meshed specimen in ANSYS (Number of nodes is 20037 and number of elements is 131443), b) Close-up nearby crack-tip

4.2. Description of Finite Element Models

Finite element code ANSYS Workbench 2021 R1 is implemented to simulate the different types of loading angle of the CTS specimen. As can be seen in Figure 4.2, mixed mode loading clevises are designed to allow the loading axis to pass through the specimen center under 0° loading angles. CTS specimen proposed by Richard [59] is used in the fracture analyses (Figure 4.2).

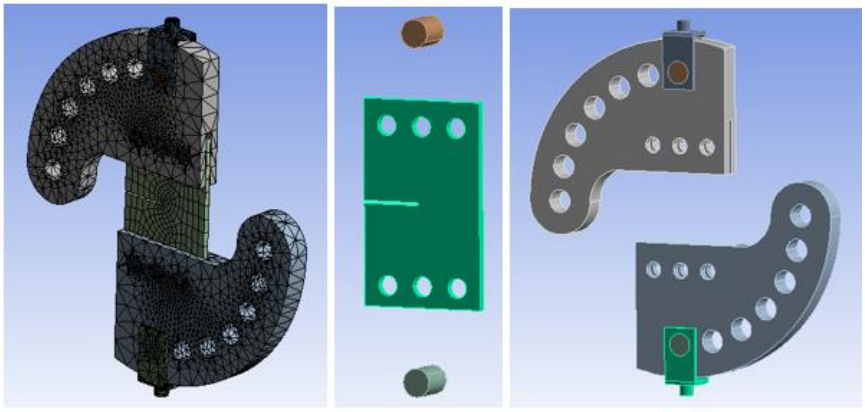

(a) (b) (c)

Figure 4.2: (a) Overall, (b) CTS specimen and Pins, and (c) Clevises views of the mixed mode-I/II model.

There are three types of cracks that can be introduced in ANSYS which are (1) Arbitrary, (2) Semielliptical, and (3) Premeshed crack. The premeshed crack method involves the crack front that

is used by the SMART Crack Growth analysis engine where the failure criterion is the stress intensity factor.

4.3. Modeling and Loading of the Specimen

Modeling and the whole assembly of the specimen is performed by SolidWorks 2021. Meshing, defining loads, boundary conditions and contacts and the solution of the problem, i.e., loading devices, pins and the specimen, with contact mechanics are performed using ANSYS 2021 R1. Also to provide the real conditions of experiments, boundary conditions are defined such that the bottom mode-I clevis surface nodes are constrained in all directions and the upper mode-I clevis surface nodes are allowed to move along loading axis only (Figure 4.3). Load is applied on the upper loading clevis. Representative picture given in Figure 4.3 is for 60° loading angle.

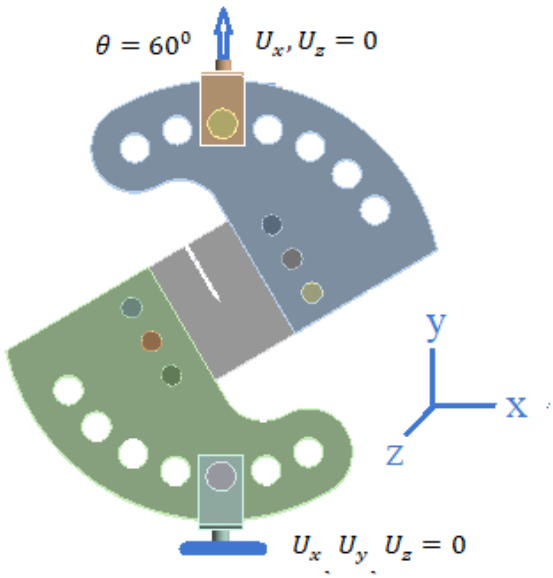

Figure 4.3: Boundary conditions and loading on mode-I/II test system – loading angle 60°.

4.4. Presence of an Initial Premeshed Crack Surface Flaw

Before any growth can be modelled, some input regarding crack dimensions and other inputs are required and an initial flaw is present in the structures. This initial flaw is usually modelled as a Premeshed surface crack in this thesis (see Figure 4.4). The previously created node sets are allocated to the crack front within the pre-mesh crack unit and the top and bottom faces of the crack. The crack coordinate system is referenced. The number of contours for solution is set to 5. These are the “loops”

through the mesh around the crack tip, which are used to evaluate the stress intensity factor by integrating the crack tip region strain energy. In the analysis the fracture mechanics method avoids the stress singularities at the crack tip. The process is repeated for the top and bottom crack faces. The new implemented feature in ANSYS is the "Smart Crack Growth" with tetrahedron mesh added after finishing the requirements of the "pre-meshed crack," in which the user can select the type of crack growth option. The mesh configuration from ANSYS for numerical determination for SIFs is showed in Figure 4.1.

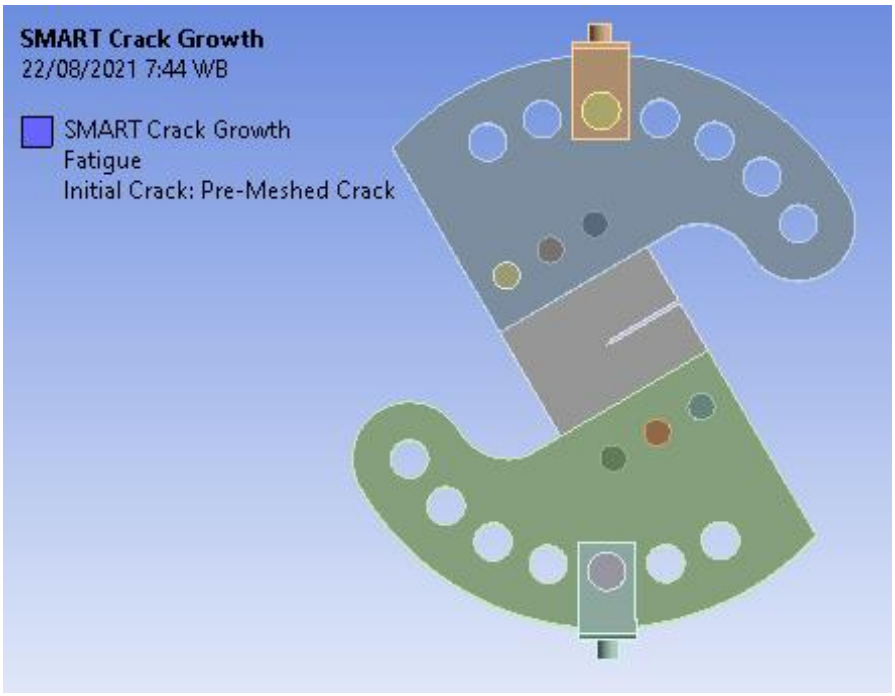

Figure 4.4: Premeshed surface crack input

CHAPTER 5

Results and Discussion

In this chapter, results from mixed mode fracture analyses are presented for different loading angles. The CAD geometry of the existing specimen are modeling and the whole assembly are performed by SolidWorks 2021 and simulations are carried out in ANSYS Workbench 2021 R1 environment. The results obtained from the model and simulation analysis are explained briefly.

The geometric dimensions of CTS specimen are shown in Figure 3.1 and the properties of the considered material, Al7075-T651 alloy are shown in Table 1. The simulation is performed under fatigue loading with the assumption that the tested material is isotropic and linear elastic. The SIFs K_I and K_{II} for all the analytical conditions were then calculated from numerical simulation of the CTS specimen under mixed-mode fatigue loading. The applied load F is decomposed into punctual loads F_1 to F_6 applied at the respective holes near the top end of the CTS specimen (See also Section 3.4), as shown in Figure 3.4. Figure 5.1 shows typical finite element meshes used for loading angle 30°, and similar meshes are used for all loading angles (45°, and 60°).

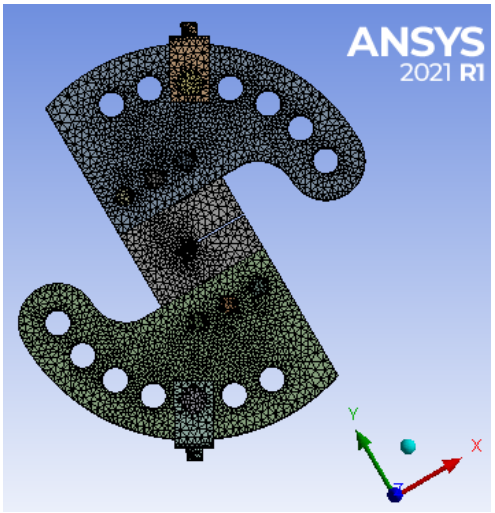

Figure 5.1: Typical finite element meshes used for FCG simulation using CTS specimen for loading angle 30°

The distribution of the maximum principal stress is shown in Figure 5.2, Figure 5.3, and **Figure 5.4** for different values of loading angles 30°, 45°, and 60° respectively.

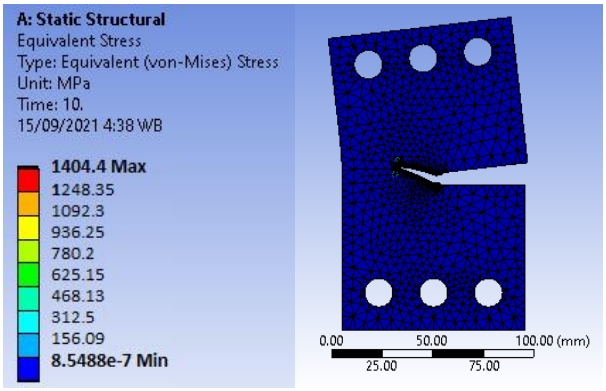

Figure 5.2: Maximum principal stress distribution with loading angle 30°

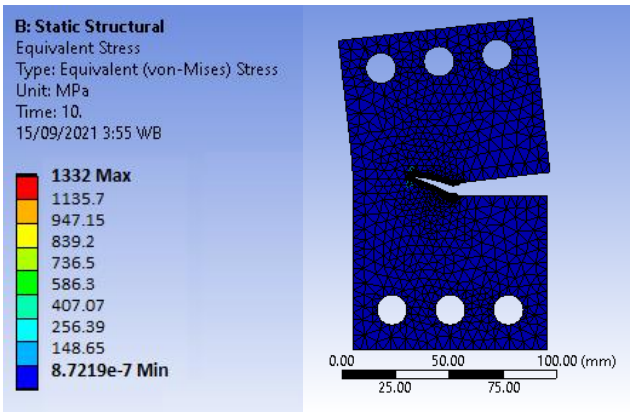

Figure 5.3: Maximum principal stress distribution with loading angle 45°

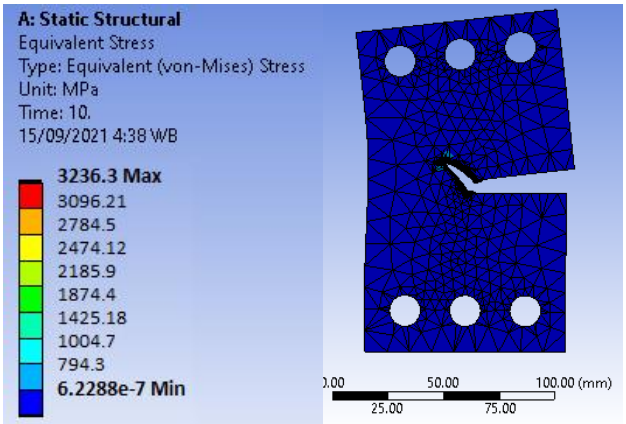

Figure 5.4: Maximum principal stress distribution with loading angle 60°

For fatigue crack growth behavior evaluation, the SIFs are important criteria. Table 4 illustrates the numerical value of SIFs obtained from the numerical simulation which were used for all numerical condition under mixed-mode fatigue loading.

Table 4: Numerical value of SIFs under mixed-mode fatigue loading.

Crack extension (mm)	30°		45°		60°	
	K_I $Mpa.m^{1/2}$	K_{II} $Mpa.m^{1/2}$	K_I $Mpa.m^{1/2}$	K_{II} $Mpa.m^{1/2}$	K_I $Mpa.m^{1/2}$	K_{II} $Mpa.m^{1/2}$
45	8.87	0.86	9.31	1.79	7.84	0.97
47	11.23	-0.63	11.8	3.64	9.67	6.99
49	13.21	4.80	12.12	3.61	11.90	5.72
51	13.23	3.79	12.9	3.73	14.95	5.97
53	13.60	1.96	14.31	4.06	17.80	6.48
55	14.39	1.79	15.52	3.94	18.86	6.59

5.1. Assessment of K_{eq} Models Using Numerical Results

This section discusses the predicted fatigue crack growth rate using selected K_{eq} models and its comparison with the experimental data performed by [24] as well as the analytical expression given by [21],[22], [23],[24], [38] for different values of loading angles $30°$, $45°$, and $60°$. These comparisons are shown in Figure 5.5-5.4 with the percentage relative error equivalent SIFs.

Figure 5.5 shows the comparisons for the variation of the crack length as a function of the corresponding K_{eq} with load angle of 30° and the amount of applied loading is $8.8\ kN$. As illustrated in this Figure 5.5 (a), the four criteria of K_{eq} agree well with the experimental tests by Demir et al. [24]. However, there is a slight divergence for all models especially at the mid of the crack length due to fatigue crack growth direction changes immediately from the pre-crack orientation. Figure 5.5 (b) show the plots of percentage relative error in predicted crack growth (with respect to the experimental K_{eq} for each of the four models for $30°$ loading angles considered in this study, estimated using the following equation (previously given as Equation 3.7). Percentage relative errors afford the error in predicted K_{eq} with respect to the experimental K_{eq} for each step of crack growth.

$$\text{Percentage relative error} = \frac{\text{Experimental } K_{eq} \; - \; \text{Predicted } K_{eq}}{\text{Experimental } K_{eq}} \times 100\%$$

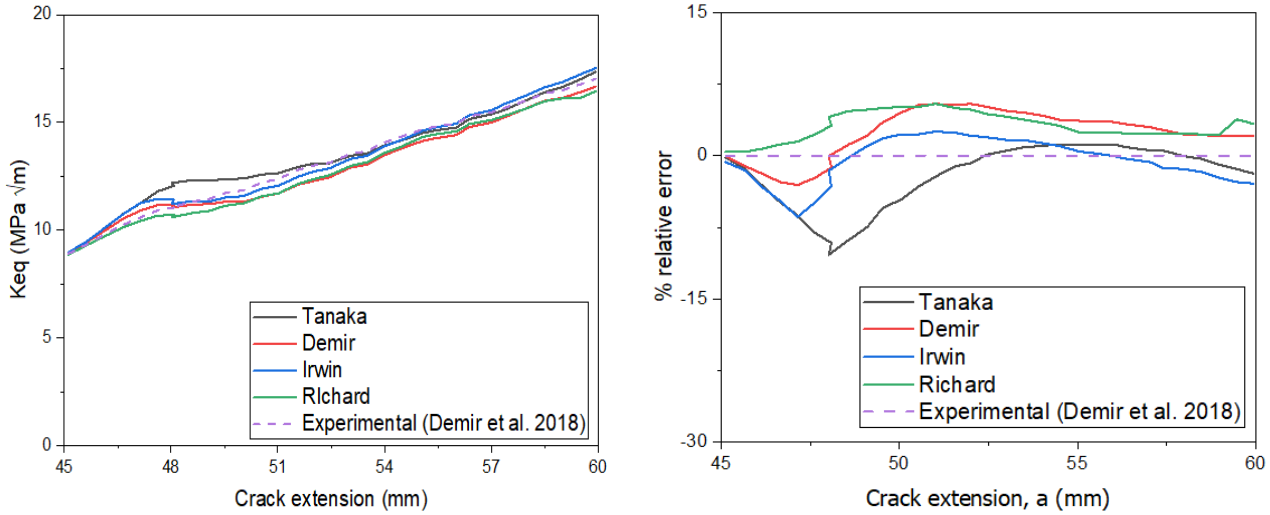

Figure 5.5: (a) Equivalent SIF with loading angle 30° (b) The percentage relative error in fatigue K_{eq} for CTS specimen of 30° loading angle.

As we can observe from Figure 5.5 (b) under 30° loading angle, all models overestimate the results at the mid of crack length. After at the mid of crack length the Tanaka model predicts equivalent stress intensity factor close to experimental results by Demir et al. [24]. However, overall, the Irwin model is predicting results consistently close to the experimental data.

In Figure 5.6, the loading angle is 45° and the amount of the load is 11.4 kN. As shown in this Figure 5.6 (a), the four criteria of K_{eq} have around the same tendency with experimental data obtained in [24]. For this loading angle even there is a slight deviation for all models from the experimental results especially at the middle of the crack extension due to fatigue crack growth direction changes instantly from the pre-crack orientation. Figure 5.6 (b) shows the percentage relative error in predicted K_{eq} (with respect to the experimental K_{eq}) for each of the four models under 45° loading angles. Generally, as shown on the Figure 5.6 (a) and (b) Tanaka's and Demir's model predicting the result close to the experimental data than the others model.

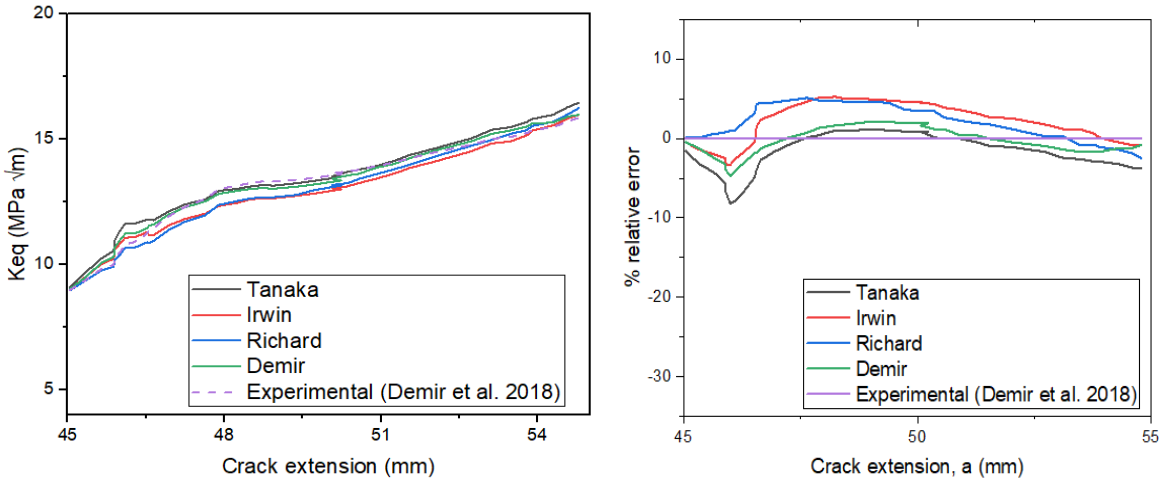

Figure 5.6: (a) Equivalent SIF with loading angle 45° (b) The percentage relative error in fatigue K_{eq} for CTS specimen of 45° loading angle.

Figure 5.7 (a) shows the comparisons for the equivalent SIF for 60° loading angle and the amount of load is $13.65\ kN$. There is clearly deviation of the initial values of the equivalent SIF for all criteria which is dependent on the initial step of the crack growth. Figure 5.7 (b) shows the percentage relative error in predicted K_{eq} (with respect to the experimental K_{eq}) for each of the four models for 60° loading angles. As we can see clearly in the Figure 5.7 (a), especially in Figure 5.7 (b), Tanaka's model overestimates the results while Demir's model predicting the results well close to the experimental results than others model.

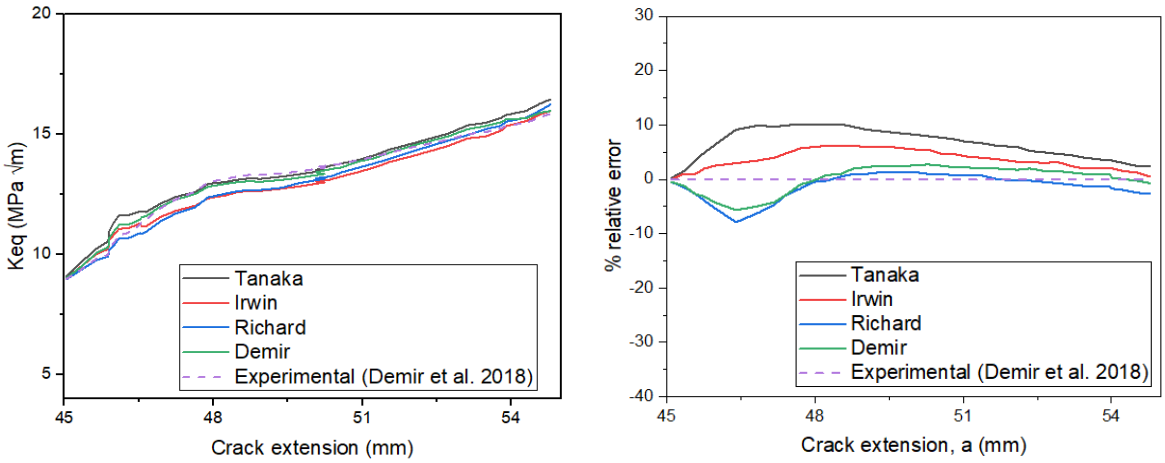

Figure 5.7: (a) Equivalent SIF with loading angle 60° (b) The percentage relative error in fatigue K_{eq} for CTS specimen of 60° loading angle.

The percentage relative error plots (Figure 5.5, Figure 5.6, and Figure 5.7) indicate that some models exhibit relatively smaller errors at the initial stages and however, at the later stages, the error is large and vice versa. Therefore, as it can be observed from the above detail results, it can be concluded that Tanaka criterion is in good agreement with the experimental results up to 45° loading angle. Although the Demir model is expected to provide higher accuracy for higher mode mixity cases, its prediction is close to the experimental data even for the case of loading angle equal to both 30° and 45°. It is evident from Figure 5.5, Figure 5.6, and Figure 5.7, taking into account the overall performance of models for the entire range of crack propagation, the K_{eq} models of Demir are predicting K_{eq} close to the experimental data compared to other K_{eq} models for all three loading angles examined in this thesis.

5.2. Fatigue Crack Growth Rate

The crack growth rate, which is used to describe the fatigue, crack propagation behavior of mechanical structures subjected to an initial crack. There exist different mathematical equations to express the relationship between the crack and growth rate. To analyze the fatigue crack growth rate of CTS specimen in this thesis the equation proposed by Erdogan and Sih [22], called Paris law (Equation 2.22, in Section 2), is used to describe the effects of equivalent SIF on the fatigue crack growth.

$$\frac{da}{dN} = C(\Delta K_{eq})^m$$

Figure 5.8-Figure 5.10 show the relationship of fatigue crack growth, da/dN with the corresponding experimental equivalent stress intensity factor using a modified formula of Paris law with loading angles of 30°, 45°, and 60° respectively. As shown from the figures, varying SIFs model also resulted in different crack growth rates across the crack front, and thus non-uniform crack propagation was seen. Because FCGR is dependent on comparable SIFs, as described in Section 4.5, it can be claimed that the Tanaka criteria is in good agreement with experimental data for fatigue crack growth rate up to 45° loading angle. By taking into account the overall performance of models, Demir's model is observed to predict crack growth rate close to experimental data. Though all models show similar trends with the experimental data, all of the models especially after $K_{eq} = 13\, MPa\sqrt{m}$ underestimate the fatigue growth rate when the sample is loaded at 60° (Figure 5.10).

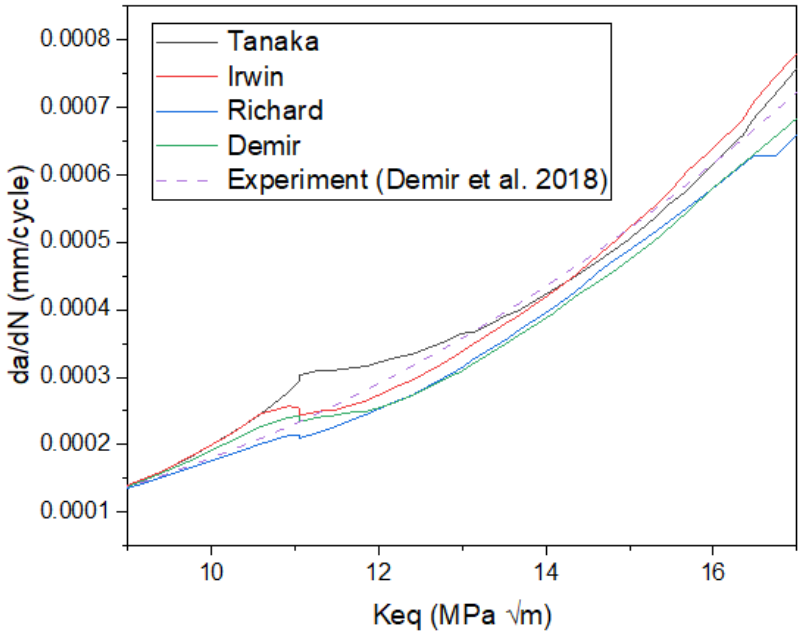

Figure 5.8: Typical crack growth curve on log-log axes with loading angle 30°

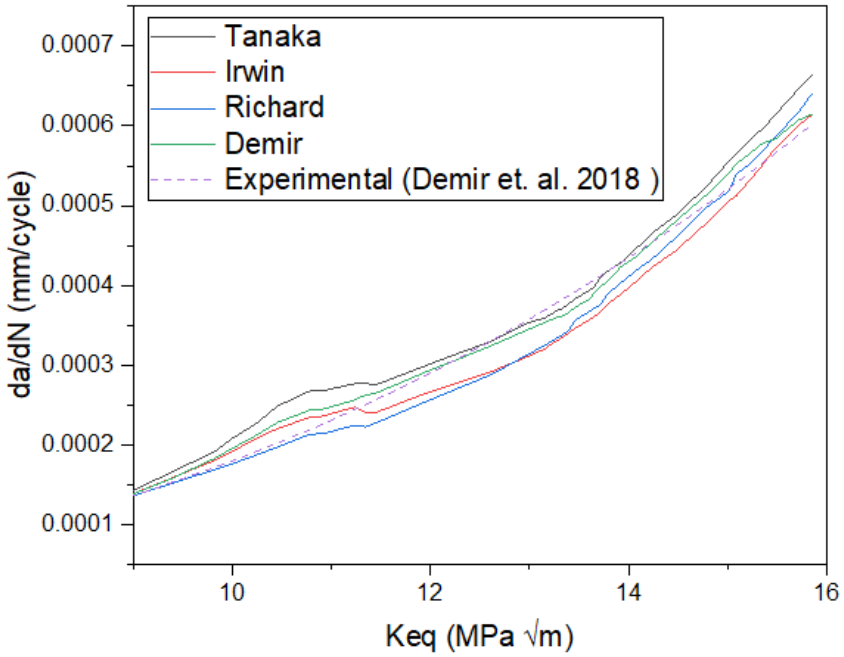

Figure 5.9: Typical crack growth curve on log-log axes with loading angle 45°

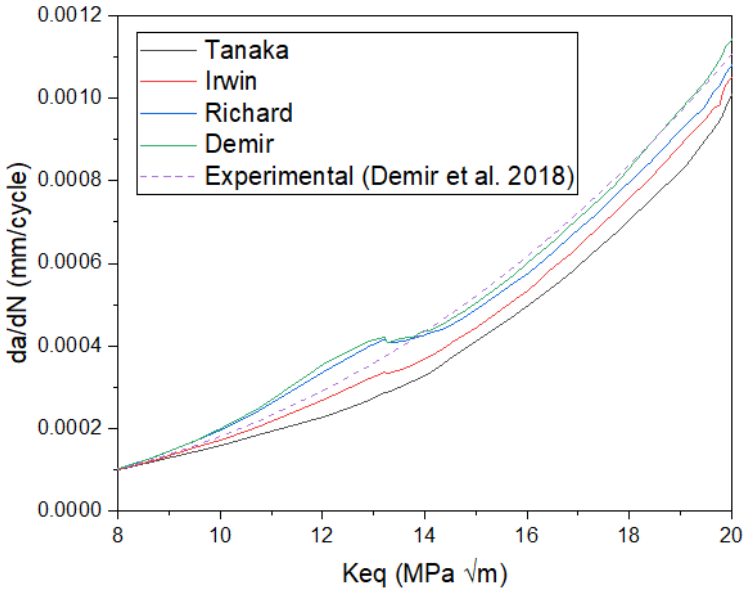

Figure 5.10: Typical crack growth curve on log-log axes with loading angle 60°

5.3. Fatigue Crack Growth Direction

Determination of the direction of crack propagation in mixed-mode loading where an opening and in-plan shear mode occur have been performed by Erdogan and Sih [22]. It is well known that the crack propagation phenomenon is highly dependent on the state of stress in the vicinity of the crack tip, therefore, SIF is considered as the most significant parameter in predicting the crack propagation path. In stress-based criteria, the MTS criterion has become one of the most commonly used criteria due to its simplicity and good agreement with the micromechanical models [45], and is employed in this thesis. This criterion states that the crack grows in a direction perpendicular to the tangential stress. The crack growth direction is obtained using the following equations, from Equations 3.9 and 3.10.

$$\theta_c = 2\,tan^{-1}\left[\frac{1}{4}\frac{K_I}{K_{II}} - \frac{1}{4}\sqrt{\left(\frac{K_I}{K_{II}}\right)^2 + 8}\,\right] \qquad \text{for} \quad K_{II} > 0$$

$$\theta_c = 2\,tan^{-1}\left[\frac{1}{4}\frac{K_I}{K_{II}} + \frac{1}{4}\sqrt{\left(\frac{K_I}{K_{II}}\right)^2 + 8}\,\right] \qquad \text{for} \quad K_{II} < 0$$

The simulation method illustrated in Section 4.2, which was proposed by Richard [60], was adopted to alleviate need for modeling the loading device. The loading arrangement and boundary conditions

imposed on the simulated specimen are shown in Figure 3.4. The force components F_1-F_6 were applied to the holes of the specimen in terms of the axial force F of the simulation are assigned as the following values (see also Section 3.4):

$$F_1 = F_6 = F(0.5\cos\alpha + \frac{c}{b}\sin\alpha)$$

$$F_2 = F_5 = F\sin\alpha, \text{ and } F_3 = F_4 = F(0.5\cos\alpha - \frac{c}{b}\sin\alpha)$$

For all the cases (30°, 45°, and 60°), the length of the pre-crack has been considered $a = 2.5\ mm$. In the first step, the fatigue pre-crack procedure has been simulated. For different loading angles, the procedure of fatigue crack growth simulation continued until the value of K_{eq} reached the fracture toughness of Al7075-T651 (i.e., $K_{IC} = 32.5\ MPa\sqrt{m}$). Then, the stress intensity was calculated using ANSYS in each node on the crack front and the maximum value of stress intensity factor was extracted and its growth direction for different loading angles were calculated using MTS criteria. As shown in Table 5, the comparison of the crack growth deflection angles are obtained using MTS criteria by substituting the maximum values of K_I and K_{II} in to Equation 3.9 and 3.10 for different loading calculated from simulation. Figure 5.11 and Figure 5.12 show predicted crack growth path and numerical crack growth paths for different loading angles respectively. It is observed that the fatigue crack growth direction changes immediately from the pre-crack orientation as the load direction changes. The SIFs output by the simulation can be used to calculate crack growth angle according to the criteria of the MTS.

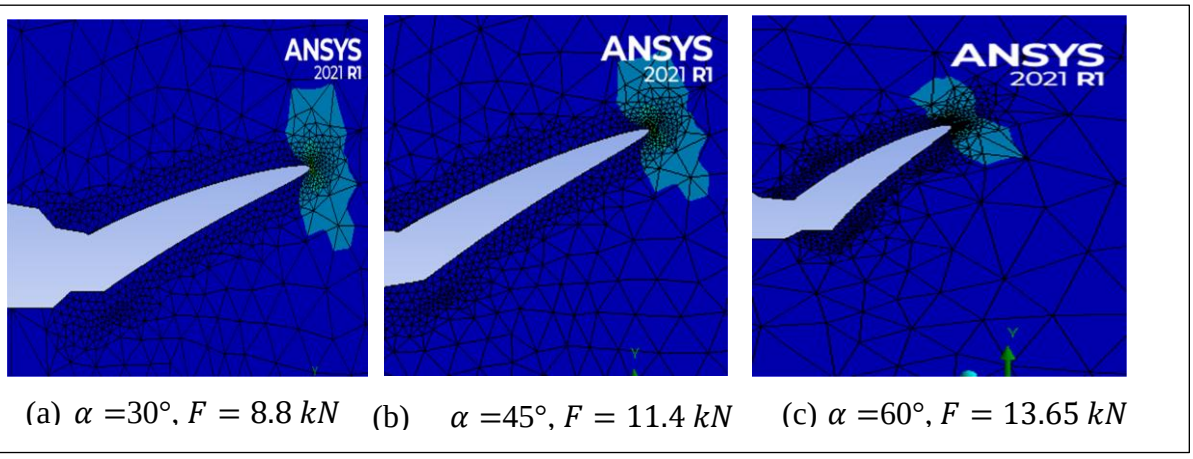

(a) α =30°, $F = 8.8\ kN$ (b) α =45°, $F = 11.4\ kN$ (c) α =60°, $F = 13.65\ kN$

Figure 5.11: Numerical crack growth paths for different loading angles

Table 5: Crack deflection angle

Loading angle, α	$F_{max}\ (N)$	$K_{I\ max}$ $(Mpa\sqrt{m})$	$K_{II\ max}$ $(Mpa\sqrt{m})$	θ_c
30°	8800	17.16	2.50	31.3°
45°	11400	15.49	3.94	47.36°
60°	13650	18.87	6.59	60.35°

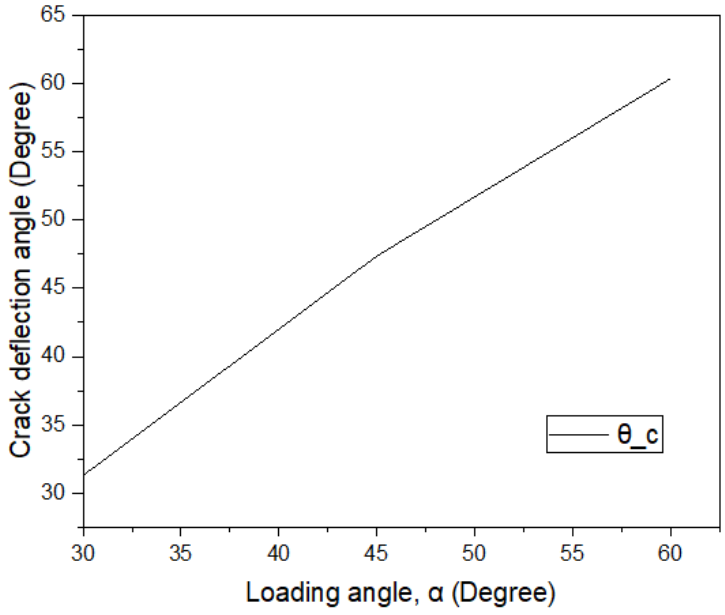

Figure 5.12: Predicted crack growth paths for several loading angles

Figure 5.13 shows the variation in K_I and K_{II} in terms of loading angle. It was drawn by using the maximum values of K_I and K_{II} with different loading angles (See Table 5) and it can be seen from the figure that, mode I is dominant in Crack deflection angle. Also it shows that when fatigue cracks are subjected to mixed-mode stress, they do not propagate in the same direction as they did before. Therefore, the equations for the SIFs (Equation 3.1 and Equation 3.2) are only valid for the straight crack, i.e., the direction of the crack does not change.

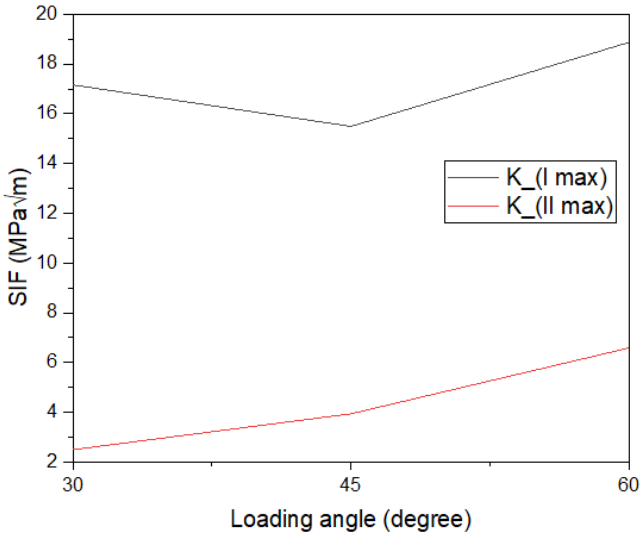

Figure 5.13: Stress intensity factors versus loading angle.

$$K_I = \frac{F}{wt}\sqrt{\pi a}\frac{\cos\alpha}{1-\frac{a}{w}}\sqrt{\frac{0.26+2.65\left(\frac{a}{w-a}\right)}{1+0.55\left(\frac{a}{w-a}\right)-0.08\left(\frac{a}{w-a}\right)^2}}$$

$$K_{II} = \frac{F}{wt}\sqrt{\pi a}\frac{\sin\alpha}{1-a/w}\sqrt{\frac{-0.23+1.40\left(\frac{a}{w-a}\right)}{1+0.67\left(\frac{a}{w-a}\right)+2.08(\frac{a}{w-a})^2}}$$

So, it is not possible to express SIFs by these equations, since the direction of fatigue crack propagation subjected to the mixed-mode loadings is deviated from its initial orientation.

CHAPTER 6

Conclusions and Recommendation

6.1. Conclusions

The primary objective of this research was to conduct mixed-mode I/II fatigue crack growth rate and path prediction using analytical and numerical methods for various equivalent stress intensity factor models under different loading angles. The loading device proposed by Richard was used to analyze the mixed mode fatigue crack growth characteristics. Then, the stress intensity factor for the actual crack length was determined using finite element analysis.

A large number of K_{eq} models have been proposed for establishing a better relationship between equivalent SIF and the crack growth rate da/dN under mixed-mode I/II loading conditions. The accuracy of the numerically estimated fatigue cracks growth rate always depends on the selected K_{eq} model. Thus this thesis attempts to assess the performances of different models for equivalent stress intensity factors in numerical prediction of crack growth curves by comparing with the same published experimental data from the literature.

Modeling and the whole assembly of the specimen are performed by SolidWorks 2021. Meshing, defining loads, boundary conditions, and contacts and the solution of the problem, i.e., loading devices, pins, and the specimen, with contact mechanics are performed using ANSYS 2021 R1. The SIFs K_I and K_{II} for all the analytical conditions were then calculated from numerical simulation of the CTS specimen under mixed-mode fatigue loading. The equivalent stress intensity factor K_{eq} has been introduced for considering mode I and mode II simultaneously.

Four models were selected to estimate the fatigue crack growth rate of CTS specimen: (1) Irwin's models, (2) Tanaka's model, (3) Richard's model, and (4) Demir's model. The results of the present investigation indicate that Tanaka criterion is in good agreement with the experimental results up to 45° loading angle. Although the Demir model is expected to provide higher accuracy for higher mode mixity cases, its prediction is close to the experimental data even for the case of loading angle equal

to both 30° and 45°. Overall, the Demir model is predicting results consistently close to the experimental data as compared to other K_{eq} models for all three loading angles examined in this thesis.

6.2. Recommendation

In this thesis, analytical and numerical modeling of fatigue crack growth behavior of CTS specimen at different loading angles was performed. Work performed in this thesis was limited to numerical and analytical analysis of a compact tension shear specimen made from a 7075-T651 Aluminum alloy in three dimensions and only four fatigue crack growth models were selected for this thesis. The varying SIFs of the models also resulted in different crack growth rates across the crack front, and thus non-uniform crack propagation was seen. Based on the outcome of this study, further investigation on the following would be sensible:

- ✓ Different procedures have been proposed to calculate the equivalent stress intensity factor, which is an important variable in order to correlate the crack behavior when a cracked structure is subjected to mixed-mode loading. Up to date, there is no standardized testing method for total fracture toughness of metals under mixed mode loading. Therefore, conducting the fatigue crack growth behavior for other SIFs model is highly recommended.
- ✓ Studying the fatigue crack growth behavior for other specimens such as double cantilever beam bonded specimens, Asymmetric three-point bending specimen, Asymmetric four-point bending specimen, Inclined cracked tension specimen, Modified Arcan specimen and fixtures, T-specimen and fixture, and for other specimens to identify which SIFs model to predict fatigue crack growth rate close experimental data.

References

[1] M. R. Nikfam, M. Zeinoddini, F. Aghebati, and A. A. Arghaei, "Experimental and XFEM modelling of high cycle fatigue crack growth in steel welded T-joints," *Int. J. Mech. Sci.*, vol. 153–154, pp. 178–193, 2019, DOI: 10.1016/j.ijmecsci.2019.01.040.

[2] S. Jiang, W. Zhang, X. Li, and F. Sun, "An Analytical Model for Fatigue Crack Propagation Prediction with Overload Effect," *Math. Probl. Eng.*, vol. 2014, 2014, DOI: 10.1155/2014/713678.

[3] H. A. Richard and M. Sander, *Fatigue Crack Growth: Detect—Assess—Avoid*, vol. 227. 2016.

[4] M. Grasso, A. De Iorio, Y. Xu, G. Haritos, M. Mohin, and Y. K. Chen, "An analytical model for the identification of the threshold of stress intensity factor range for crack growth," *Adv. Mater. Sci. Eng.*, vol. 2017, 2017, DOI: 10.1155/2017/3014172.

[5] T. l. Anderson, *Fracture Mechanics: Fundamental and Application*, Fourth. Taylor & Francis, 2017.

[6] M. T. Shridharmurthy H N, H K Srinivas, Shashidhara L C, "a Review on Investigation of Mixed Mode Fracture in Brittle Materials," *Int. J. Res. Eng. Technol.*, vol. 05, no. 21, pp. 24–29, 2016, DOI: 10.15623/ijret.2016.0521005.

[7] O. Demir, A. O. Ayhan, and S. İriç, "A new specimen for mixed mode-I/II fracture tests: Modeling, experiments and criteria development," *Eng. Fract. Mech.*, vol. 178, pp. 457–476, 2017, DOI: 10.1016/j.engfracmech.2017.02.019.

[8] L. Stepanova, "Computational and experimental study of mixed mode loading of the cracked semi-circular disc under bending," *J. Phys. Conf. Ser.*, vol. 1368, no. 4, 2019, DOI: 10.1088/1742-6596/1368/4/042066.

[9] P. Zhang, L. qi Xie, C. yu Zhou, and X. hua He, "Experimental and numerical investigation on fatigue crack growth behavior of commercial pure titanium under I-II mixed mode loading at negative load ratios," *Int. J. Fatigue*, vol. 138, p. 105700, 2020, DOI: 10.1016/j.ijfatigue.2020.105700.

[10] Y. Wang, W. Wang, B. Zhang, and C. Q. Li, "A review on mixed mode fracture of metals," *Eng. Fract. Mech.*, vol. 235, no. April, p. 107126, 2020, DOI: 10.1016/j.engfracmech.2020.107126.

[11] E. E. Gdoutos, "Mixed-mode crack growth predictions," *Eng. Fract. Mech.*, vol. 28, no. 2, pp. 211–221, 1987, DOI: 10.1016/0013-7944(87)90215-3.

[12] L. Nash Gifford and P. D. Hilton, "Stress intensity factors by enriched finite elements," *Eng. Fract. Mech.*, vol. 10, no. 3, pp. 485–496, 1978, DOI: 10.1016/0013-7944(78)90059-0.

[13] S. T. Raveendra and P. K. Banerjee, "Boundary element analysis of cracks in thermally stressed planar structures," *Int. J. Solids Struct.*, vol. 29, no. 18, pp. 2301–2317, 1992, DOI: 10.1016/0020-7683(92)90217-H.

[14] T. Belytschko and T. Black, "Elastic Crack Growth in Finite Elements with Minimal Remeshing," *Int. J. Numer. Methods Eng.*, vol. 124, no. 18, pp. 601–620, 1999, DOI: 10.3760/cma.j.issn.0366-6999.2011.18.023.

[15] N. Moës, J. Dolbow, and T. Belytschko, "A finite element method for crack growth without remeshing," *Int. J. Numer. Methods Eng.*, vol. 46, no. 1, pp. 131–150, 1999, DOI: 10.1002/(SICI)1097-0207(19990910)46:1<131::AID-NME726>3.0.CO;2-J.

[16] K. Nasri and M. Zenasni, "Fatigue crack growth simulation in coated materials using X-FEM," *Comptes Rendus - Mec.*, vol. 345, no. 4, pp. 271–280, 2017, DOI: 10.1016/j.crme.2017.02.005.

[17] K. Rege and H. G. Lemu, "A review of fatigue crack propagation modelling techniques using FEM and XFEM," in *IOP Conference Series: Materials Science and Engineering*, 2017, vol. 276, no. 1, DOI: 10.1088/1757-899X/276/1/012027.

[18] X. Miao *et al.*, "Numerical Simulation of Mixed-Mode Fatigue Crack Growth for Compact Tension Shear Specimen," *Adv. Mater. Sci. Eng.*, vol. 2020, no. 2019, p. 102647, 2020, DOI: 10.1155/2020/5426831.

[19] Y. A. Fageehi and A. M. Alshoaibi, "Numerical Simulation of Mixed-Mode Fatigue Crack Growth for Compact Tension Shear Specimen," *Adv. Mater. Sci. Eng.*, vol. 2020, 2020, DOI: 10.1155/2020/5426831.

[20] I. ANSYS, "SMART Fracture," *Ansys*, pp. 1–22, 2020.

[21] G. R. Irwin, "Analysis of stresses and strains near the end of a crack traversing a plate." Journal of Applied Mechanics, pp. 361–364, 1957.

[22] F. Erdogan and G. C. Sih, "On the crack extension in plates under plane loading and transverse shear," *J. Fluids Eng. Trans. ASME*, vol. 85, no. 4, pp. 519–525, 1963, DOI: 10.1115/1.3656897.

[23] K. Tanaka, "Fatigue crack propagation from a crack inclined to the cyclic tensile axis," *Eng. Fract. Mech.*, vol. 6, no. 3, 1974, DOI: 10.1016/0013-7944(74)90007-1.

[24] O. Demir, A. O. Ayhan, S. Iric, and H. Lekesiz, "Evaluation of mixed mode-I/II criteria for fatigue crack propagation using experiments and modeling," *Chinese J. Aeronaut.*, vol. 31, no. 7, pp. 1525–1534, 2018, DOI: 10.1016/j.cja.2018.05.009.

[25] M. S. A. H. and A. K. A. Abdulnaser M Alshoaibi, "Finite Element Simulation of Fatigue Life Estimation and Crack Path Prediction of Two- dimensional Structures Components," no. August 2015, 2013, DOI: 10.1080/1023697X.2008.10668103.

[26] K. P. Wolff, R. L. S. Pitangueira, and R. G. Peixoto, "A displacement-based and explicit non-planar 3D crack propagation model in the generalized/extended finite element method," *Theor. Appl. Fract. Mech.*, vol. 108, p. 102647, 2020, DOI: 10.1016/j.tafmec.2020.102647.

[27] R. O. Ritchie, "Mechanisms of fatigue-crack propagation in ductile and brittle solids," *Int. J. Fract.*, vol. 14, no. 2, pp. 111–117, 1999, DOI: 10.1088/1009-0630/14/2/06.

[28] M. F. K. and C. L. Popelar, *Advanced fracture mechanics*, 1st ed. New York: Oxford University Press, 1985.

[29] A. Carpinteri, F. Berto, G. Fortese, C. Ronchei, D. Scorza, and S. Vantadori, "Modified two-parameter fracture model for bone," *Eng. Fract. Mech.*, vol. 174, pp. 44–53, 2017, DOI: 10.1016/j.engfracmech.2016.11.002.

[30] A. M. A. Mageed and R. K. Pandey, "Mixed mode crack growth under static and cyclic loading in A1-alloy sheets," *Eng. Fract. Mech.*, vol. 40, no. 2, pp. 371–385, 1991, DOI: 10.1016/0013-

7944(91)90271-2.

[31] M. A. Hussain, S. L. Pu, and J. Underwood, "Strain Energy Release Rate for a Crack Under Combined Mode I and Mode II," in *Fracture Analysis: Proceedings of the 1973 National Symposium on Fracture Mechanics, Part II*, G. R. Irwin, Ed. West Conshohocken, PA: ASTM International, 1974, pp. 2–28.

[32] G. C. Sih, "Strain-energy-density factor applied to mixed mode crack problems," *Int. J. Fract.*, vol. 10, no. 3, pp. 305–321, 1974, DOI: 10.1007/BF00035493.

[33] A. Y. Elruby, S. Nakhla, and A. Hussein, "Automating XFEM Modeling Process for Optimal Failure Predictions," *Math. Probl. Eng.*, vol. 2018, 2018, DOI: 10.1155/2018/1654751.

[34] H. A. Richard, A. Eberlein, and G. Kullmer, "Concepts and experimental results for stable and unstable crack growth under 3D-mixed-mode-loadings," *Eng. Fract. Mech.*, vol. 174, pp. 10–20, 2017, DOI: 10.1016/j.engfracmech.2016.12.005.

[35] D. Rozumek and E. MacHa, "A survey of failure criteria and parameters in mixed-mode fatigue crack growth," *Mater. Sci.*, vol. 45, no. 2, pp. 190–210, 2009, DOI: 10.1007/s11003-009-9179-2.

[36] K. Walker, "The Effect of Stress Ratio During Crack Propagation and Fatigue for 2024-T3 and 7075-T6 Aluminum," in *Effects of Environment and Complex Load History on Fatigue Life*, M. S. Rosenfeld, Ed. West Conshohocken, PA: ASTM International, 1970, pp. 1–14.

[37] "Fracture Mechanics and Fatigue Crack Growth Analysis Software Terms and License Agreement May 2019 Code Capabilities NASGRO Availability & Licensing Philosophy Multiple Installations & Site License Payment Terms , Delivery and Installation SwRI Contact In," no. May, 2019.

[38] M. Schöllmann, H. A. Richard, G. Kullmer, and M. Fulland, "A new criterion for the prediction of crack development," *Int. J. Fract.*, vol. 117, pp. 129–41, 2002.

[39] H. C. Rhee, "Fatigue crack growth analyses of offshore structural tubular joints," *Eng. Fract. Mech.*, vol. 34, no. 5–6, pp. 1231–1239, 1989, DOI: 10.1016/0013-7944(89)90283-X.

[40] J. Qian and A. Fatemi, "Mixed mode fatigue crack growth: A literature survey," *Eng. Fract. Mech.*, vol. 55, no. 6, pp. 969–990, 1996, DOI: 10.1016/S0013-7944(96)00071-9.

[41] J. Chang, J. Q. Xu, and Y. Mutoh, "A general mixed-mode brittle fracture criterion for cracked materials," *Eng. Fract. Mech.*, vol. 73, no. 9, pp. 1249–1263, 2006, DOI: 10.1016/j.engfracmech.2005.12.011.

[42] Q. Wang, X. Liu, W. Wang, C. Yang, X. Xiong, and H. Fang, "Mixed mode fatigue crack growth behavior of Ni-Cr-Mo-V high strength steel weldments," *Int. J. Fatigue*, vol. 102, pp. 79–91, 2017, DOI: 10.1016/j.ijfatigue.2017.05.001.

[43] S. Qi, L. X. Cai, C. Bao, H. Chen, K. K. Shi, and H. L. Wu, "Analytical theory for fatigue crack propagation rates of mixed-mode I–II cracks and its application," *Int. J. Fatigue*, vol. 119, no. October 2018, pp. 150–159, 2019, DOI: 10.1016/j.ijfatigue.2018.10.004.

[44] A. M. Abdel Mageed and R. K. Pandey, "Studies on cyclic crack path and the mixed-mode crack closure behaviour in Al alloy," *Int. J. Fatigue*, vol. 14, no. 1, pp. 21–29, 1992, DOI: 10.1016/0142-1123(92)90149-7.

[45] D. Salimi-Majd, F. Shahabi, and B. Mohammadi, "Effective local stress intensity factor criterion for prediction of crack growth trajectory under mixed mode fracture conditions," *Theor. Appl. Fract. Mech.*, vol. 85, pp. 207–216, 2016, DOI: 10.1016/j.tafmec.2016.01.009.

[46] S. K. Chan, I. S. Tuba, and W. K. Wilson, "On the finite element method in linear fracture mechanics," *Eng. Fract. Mech.*, vol. 2, no. 1, pp. 1–17, Jul. 1970, DOI: 10.1016/0013-7944(70)90026-3.

[47] E. Byskov, "The calculation of stress intensity factors ssing the finite element method with cracked elements," *Int. J. Fract.*, vol. 26, no. 4, pp. 329–337, 1970, DOI: 10.1007/BF00962965.

[48] W. K. Wilson, "Finite element methods for elastic bodies containing cracks," *Methods Anal. Solut. crack Probl.*, pp. 484–515, 1973, DOI: 10.1007/978-94-017-2260-5_9.

[49] R. H. Hardy, "A high-order finite element model for acoustic propagation," 1974, [Online]. Available: https://eprints.soton.ac.uk/400677/.

[50] A. Holston, "A mixed mode crack tip finite element," *Int. J. Fract.*, vol. 12, no. 6, pp. 887–899, 1976, DOI: 10.1007/BF00034626.

[51] C. P. Jiang and Y. K. Cheung, "A special bending crack tip finite element," *Int. J. Fract.*, vol. 71, no. 1, pp. 57–69, 1995, DOI: 10.1007/BF00019341.

[52] J. D. Eshelby, "The Continuum Theory of Lattice Defects," *Solid State Phys. - Adv. Res. Appl.*, vol. 3, no. C, pp. 79–144, 1956, DOI: 10.1016/S0081-1947(08)60132-0.

[53] D. Broek and J. R. Rice, "Elementary Engineering Fracture Mechanics," *Journal of Applied Mechanics*, vol. 42, no. 3. pp. 751–752, 1975, DOI: 10.1115/1.3423697.

[54] J.R.Rice, "'A Path Independent Integral and the Approximate Analysis of Strain Concentration by Notches and Cracks,'" *J. Appl. Mech.*, vol. 35, no. 2, p. 379, 1968.

[55] E. F. Rybicki and M. F. Kanninen, "A finite element calculation of stress intensity factors by a modified crack closure integral," *Eng. Fract. Mech.*, vol. 9, no. 4, pp. 931–938, 1977, DOI: 10.1016/0013-7944(77)90013-3.

[56] J. Shi, D. Chopp, J. Lua, N. Sukumar, and T. Belytschko, "Abaqus implementation of extended finite element method using a level set representation for three-dimensional fatigue crack growth and life predictions," *Eng. Fract. Mech.*, vol. 77, no. 14, pp. 2840–2863, 2010, DOI: 10.1016/j.engfracmech.2010.06.009.

[57] J. Remacle, J. Lambrechts, and B. Seny, "Blossom-Quad: A non-uniform quadrilateral mesh generator using a minimum-cost perfect-matching algorithm," *International*, no. February, pp. 1102–1119, 2012, DOI: 10.1002/nme.

[58] R. M. Chlistovsky, P. J. Heffernan, and D. L. DuQuesnay, "Corrosion-fatigue behaviour of 7075-T651 aluminum alloy subjected to periodic overloads," *Int. J. Fatigue*, vol. 29, no. 9–11, pp. 1941–1949, 2007, DOI: 10.1016/j.ijfatigue.2007.01.010.

[59] H. A. Richard and K. Benitz, "A loading device for the creation of mixed mode in fracture mechanics," *Int. J. Fract.*, vol. 22, no. 2, pp. 55–58, 1983, DOI: 10.1007/BF00942726.

[60] M. Sander and H. A. Richard, "Experimental and numerical investigations on the influence of

the loading direction on the fatigue crack growth," vol. 28, pp. 583–591, 2006, DOI: 10.1016/j.ijfatigue.2005.05.012.

[61] A. R. Shahani, I. Shakeri, and C. D. Rans, "Fatigue crack growth of Al 5083-H111 subjected to mixed-mode loading," *J. Brazilian Soc. Mech. Sci. Eng.*, vol. 42, no. 8, 2020, DOI: 10.1007/s40430-020-02527-8.

[62] H. A. Richard, M. Fulland, and M. Sander, "Theoretical crack path prediction," *Fatigue Fract. Eng. Mater. Struct.*, vol. 28, no. 1–2, pp. 3–12, 2005, DOI: 10.1111/j.1460-2695.2004.00855.x.